Interpretation of normal-deformed bands in ^{167}Lu

Azam Kardan,[1,*] Ingemar Ragnarsson,[2,†] B. Gillis Carlsson,[2] and Hai-Liang Ma[3]
[1]*School of Physics, Damghan University, P.O. Box 36716-41167, Damghan, Iran*
[2]*Division of Mathematical Physics, LTH, Lund University, P.O. Box 118, SE-221 00 Lund, Sweden*
[3]*China Institute of Atomic Energy, P.O. Box 275-10, Beijing 102413, China*

(Received 7 October 2019; published 30 January 2020)

With the aim to get a general understanding of rotational bands in the deformed rare-earth region or in deformed nuclei in general, the observed normal-deformed rotational structures in ^{167}Lu are interpreted within the unpaired and paired cranked Nilsson-Strutinsky formalisms, cranked Nilsson-Strutinsky and cranked Nilsson-Strutinsky-Bogoliubov. Particular attention is devoted to the band crossings. For this nucleus with the Fermi surface high up in the $h_{11/2}$ shell, we conclude that except for the paired AB and BC crossings in configurations with an even and odd number of $i_{13/2}$ neutrons, respectively, the observed band crossings can be understood within the unpaired formalism. Especially, it means that above the AB and BC crossings, the evolution with spin is described as a gradual alignment of the spin vectors of the particles outside closed shells. Consequently, the configurations can be characterized by the number of particles occupying open j shells or groups of j shells. In the present study, we revise the interpretation of some experimental bands and also the nature of the crossings while some previous configuration assignments are confirmed.

DOI: 10.1103/PhysRevC.101.014323

I. INTRODUCTION

In the analysis of nuclear high-spin states, much emphasis has been put on band crossings caused by alignments of high-j particles. Such band crossings are formed when the Coriolis and centrifugal forces overcome the pairing forces which try to keep the particles in time-reversed orbitals. Specifically, after the discovery of the backbending phenomenon almost 50 years ago [1], it was soon realized that it was caused by this type of band crossings [2]. Subsequently, with the assumption that it is a reasonable approximation to assume that the deformation and the pairing gap stay constant over the crossing region, a simple and illustrative formalism [3,4], the cranked shell model (CSM) was developed in Copenhagen. This formalism has been very successful to explain, e.g., the details of the first crossing in the rare-earth region, caused by the $i_{13/2}$ neutrons, and generally also to describe the second crossing in these nuclei caused by the $h_{11/2}$ protons; see, e.g., Refs. [5,6].

When going to higher spin values, the Coriolis and centrifugal forces will lead to shape changes and configuration changes not accounted for by the CSM in its standard form. With the purpose to treat these features in detail the so called cranked Nilsson-Strutinsky (CNS) formalism [7] was developed. The main purpose of this formalism is to describe high and very high spin states, where pairing correlations are assumed to be of minor importance and are therefore neglected. In both the CSM and CNS formalisms, diabatic configurations are followed through band-crossings, where computer codes are used in the CNS formalism to do this in a systematic way over the entire deformation space. With some further developments of the formalism [8,9], it is now possible to fix configurations in a detailed way based on the occupation of $\mathcal{N}$ shells, and of j shells or groups of j shells within each $\mathcal{N}$ shell.

With the background of the CNS model, the ultimate cranker model was developed in the late 1980s [10,11]. In this model, it is in principle possible to follow diabatic configurations and carry out self-consistent calculations in both pairing space and deformation space. However, this requires heavy computer calculations which were very difficult not to say impossible to carry through in the early years of the model. Even so, already at the introduction of the ultimate cranker, attempts were made to follow the deformation changes and the decrease of pairing in the rotational bands in ^{158}Er when they approach termination in the $I > 40\hbar$ spin range [11]. Furthermore, for the superdeformed bands in ^{143}Eu, the details of the decrease of pairing with increasing angular momentum have been investigated [12].

The mentioned studies on ^{158}Er and ^{143}Eu are, however, rather exceptions and the ultimate cranker has mainly been used to apply the CSM formalism. Configurations are then labeled by the number of aligned particles; see, e.g., Ref. [13] and references therein. In our view, this becomes questionable when going beyond the first and maybe second band-crossing because pairing is then severely quenched and it is not meaningful to make a division into spin vectors which are aligned and those which are not aligned. Indeed, when the CSM model was introduced [3,4] it was clearly stated that it was mainly intended for the understanding of rotating deformed nuclei up to an angular momentum of about $30\hbar$.

The possibility to get a detailed understanding of very high spin states has been demonstrated in the CNS model

*Corresponding author: aakardan@du.ac.ir
†ingemar.ragnarsson@matfys.lth.se

but mainly on nuclei where it has been possible to follow configurations which reach or come close to termination and on superdeformed states. Thus, examples of successful studies of high-spin level schemes within the CNS formalism are spread over the nuclear periodic table, e.g., ^{20}Ne [14] and ^{38}Ar [15] where strongly deformed bands have been followed to termination, ^{62}Zn where the excitation of p-h excitations can be followed from the ground state to superdeformation [16], ^{74}Kr [17] where a band is followed to an $I_{\max}$ state which is still collective, ^{109,110}Sb [8,18] with a detailed prediction of smooth terminating states, ^{113}I [19] where experiment is coming close to a very high spin state which terminates high above yrast, the superdeformed bands in the ^{152}Dy region [20] and ^{157,158}Er [21,22] with a detailed understanding not only of the high-spin terminations but, for ^{157}Er, also of the feeding of the terminating states.

A few years ago, the ultimate cranker formalism was updated so that it is now straightforward to make calculations in a mesh covering both the deformation space and pairing space, the cranked Nilsson-Strutinsky-Bogoliubov (CNSB) formalism [23,24]. Combined with the CNS formalism and its possibility to label configurations in detail, this leads to a very powerful formalism to analyze high-spin states. Here we will test this formalism on a nucleus in the middle of the deformed rare-earth region, namely, on ^{167}Lu where one of the most extensive level schemes in this region of nuclei has recently been published, see Ref. [13]. The high-spin states in Lu nuclei are particularly interesting since it is in these isotopes that one has observed [25–28] the nuclear wobbling excitation. Observation of the wobbling mode gives firm evidence that nuclei are triaxial and shows to what degree nuclei can be seen as rigid triaxial bodies. While several articles have been devoted solely to the study of the wobbling mode, ours is the first detailed study of the remaining states and shows how well theory can describe the states of this nucleus. The nucleus ^{167}Lu is of special interest because it is the only case where an interaction has been observed at high spin between the normal-deformed states and the wobbling band. Note also that, mainly because of the wobbling excitations identified in this region of nuclei, extensive level schemes have been published for many neighboring nuclei; see, e.g., Refs. [29–34].

In Ref. [13], the standard procedure was followed, assuming that, with increasing angular momentum, the different rotational bands can be characterized by an increasing number of particles that have their spin vectors aligned. As mentioned above we do not find such a description meaningful for very high spin states, say $I > 30$ in the deformed rare earth region. Indeed, our calculations below show that such high-spin bands in ^{167}Lu are well understood from configurations with a fixed number of particles in different (groups of) j shells where the spin vectors of the valence particles become gradually more and more aligned with increasing rotational frequency. We believe that these results are of a more general nature, where similar conclusions can be drawn from our previous studies of ^{161}Lu [24] which is rather a transitional nucleus in the outskirts of the deformed rare earth region.

The observed bands of ^{167}Lu are analyzed in Sec. II where special emphasis is put on interactions between different bands. Our theoretical models, CNS and CNSB, are briefly described in Sec. III. The observed bands are then analyzed in these models in Sec. IV and configurations are assigned to the different bands. Finally, our results are summarized in Sec. V with some brief suggestions for future experiments. In the Appendix, we discuss how the alignment at band crossings should be defined and how this alignment can be determined for observed rotational bands.

II. EXPERIMENTAL BANDS AND THEIR LABELING

The experimental positive and negative parity bands in ^{167}Lu are drawn in Figs. 1(a) and 1(b), respectively. They are taken from Ref. [13], where they are all labeled with a number and in most cases also with one or several letters referring to which orbitals are considered aligned. However, as discussed below, in some cases, we define bands in a different way; e.g., when two bands interact we try to form smooth undisturbed crossing bands. Thus, we have added labels on some of the bands referring to our interpretation. For such bands we will mainly use these labels, defined in Fig. 1, when comparing with calculations, while for other bands, we will use the original labels of Ref. [13]. In our labels, the letter a is used for signature $\alpha = 1/2$ bands and b for $\alpha = -1/2$ bands.

Consider first the positive parity bands. As discussed in connection with band 10 in Ref. [13], there is a crossing between bands 1 and 10 at $I \approx 30$. Furthermore, there appears to be a crossing between band 9a and the TSD1 band, also at $I \approx 30$. These crossings will be discussed in detail below and we will conclude that the crossing bands at the yrast line should be assigned as [404]7/2 and a three-quasiparticle configuration with 7 $h_{11/2}$ protons and 5 $i_{13/2}$ neutrons (labeled as 404h). Furthermore, in agreement with Ref. [13], the band labeled 4 is interpreted as a three-quasiparticle configuration.

For negative parity, the low spin range of band 15 is built on the $h_{11/2}$ orbital where it turns out to be somewhat questionable if it is the [523]7/2 or the [514]9/2 orbital which is involved. Thus, we will refer to it as the $h_{11/2}$ band. The bands 13 and 14 appear to be associated with the [541]1/2 orbital. Thus, we will sometimes refer to these bands as the 541 bands. Bands 2 and 3 are assigned as three-quasiparticle bands in agreement with Ref. [13].

Bands 6 and 7 are rather short but we will give some comments on them in Sec. IV A, while band 5 is too short to make it meaningful to suggest any assignment. The spin and parity of band 16 is uncertain. However, with the values suggested in Ref. [13] and used in Fig. 1(b), the E versus I curve of the band becomes similar to that of bands 13 and 3. This indicates that the values in Ref. [13] are correct because with other values, the band would become too different compared with the other observed bands. We will give some short comments on this band in Sec. IV C.

Bands 11 and 12 are generally labeled as triaxial strongly deformed, TSD1 and TSD2, with similar bands observed in ^{163,165}Lu [26,27]. The structure of the TSD1 bands is accepted since long, see Refs. [35–38]. The TSD2 bands are understood as a wobbling excitation built on the TSD1 bands; see Refs. [37,39–43]. However, using similar methods as employed here, it has recently been pointed out [44] that

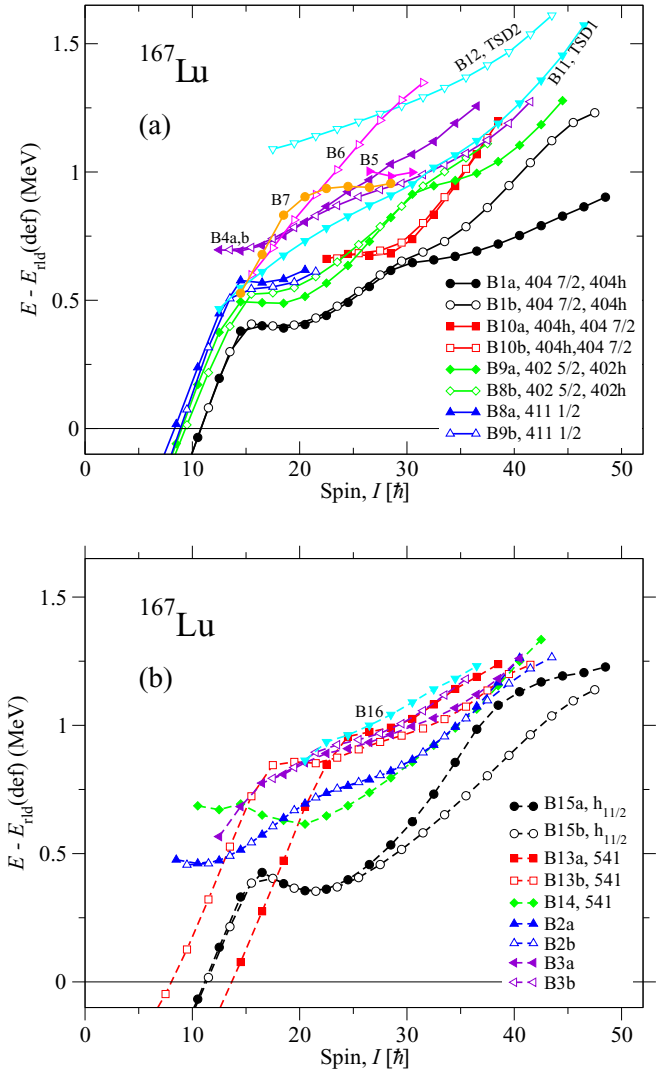

FIG. 1. Energies of the experimental (a) positive and (b) negative parity bands in ^{167}Lu. The bands are labeled by the numbers used in Ref. [13], but for some bands we define different labels which are also given and which are used in our interpretation. For the proton bands based on the $\mathcal{N} = 4$ orbitals, see also Fig. 4 below. The negative parity orbitals interpreted as built on an $h_{11/2}$ or on the [541]1/2 hf orbital are labeled as $h_{11/2}$ and 541, respectively. The positive (negative) parity bands are drawn by full (dashed) lines while closed (open) symbols are used for signature $\alpha = 1/2$ $(-1/2)$ bands. This convention is used for all figures.

there are some problems with the interpretation that these bands are formed in a strongly deformed triaxial minimum. Here, we will add some comments on how the TSD1 band interacts with the normal-deformed bands but we have nothing to add on the interpretation of these "TSD" bands.

A. Band crossings—Smooth undisturbed bands

A closer study of the energy-level scheme in Fig. 1(a) indicates an interesting sequence of interactions between the positive parity structures. Observed transitions which link the bands are shown by arrows in Figs. 2(a) and 2(b), which are

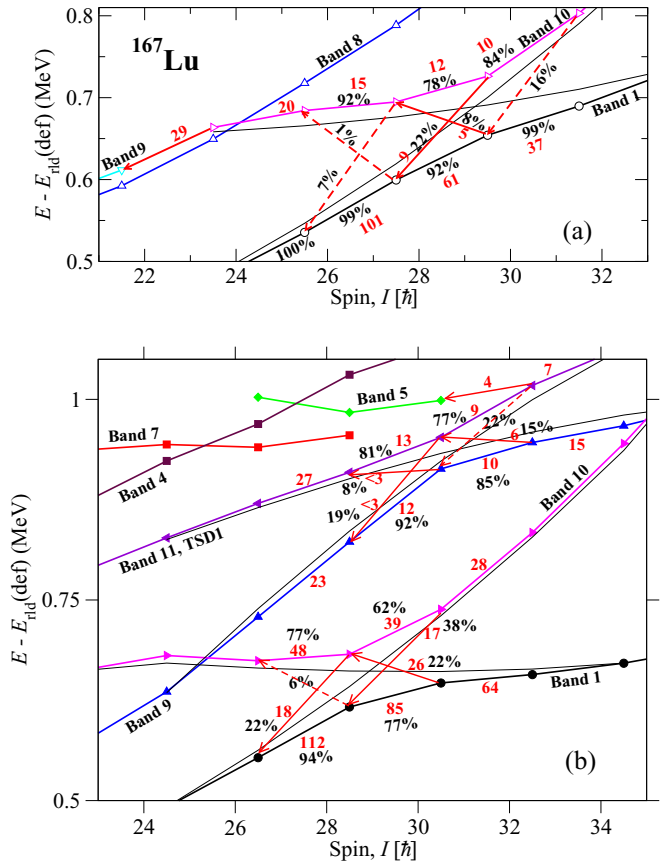

FIG. 2. Blown ups of Fig. 1(a) in the spin region where the transitions are observed between (a) bands 10 and 1 for $\alpha = -1/2$ and (b) bands 10 and 1, and bands 9 and 11 for $\alpha = +1/2$. Thin lines are used for crossing bands fitted in two-band-mixing calculations; see Sec. II A. Observed transitions are shown by solid line red arrows while dashed arrows are used for transitions that are not observed. Experimental intensities are written in red while calculated branching ratios are given in percentage by black numbers.

blow ups of Fig. 1(a) for signature $\alpha = -1/2$ and $1/2$, respectively, in the spin region where the transitions are observed.

Specifically, both the odd and the even spin sequences of bands 1 and 10 interact around $I = 30$ where they come close together. It suggests that bands 1 and 10 cross and exchange character at $I \approx 30$. Thus, in a similar way as was previously done for ^{76}Rb [45], we have performed a two-band-mixing calculation to find out if this scenario is consistent with the observed bands. In this calculation, two smooth unperturbed bands are parameterized with a constant moment of inertia. They interact with strengths which are assumed to be constant over the spin range $I = 23.5$–33.5 ($I = 24.5$–34.5) for the $\alpha = -1/2$ ($\alpha = 1/2$) bands. With a least-square fit, all observed states in this spin range are reproduced within ± 7 (± 5) keV with an interaction matrix element of 38 keV (30 keV). As seen in Fig. 2 the two undisturbed bands cross at $I \approx 29$ for both signatures. The interaction between bands 1 and 10 is also discussed in Ref. [13], where, in general agreement with the present fit, a maximum interaction strength of $|V_{\max}| = 33$ keV is deduced.

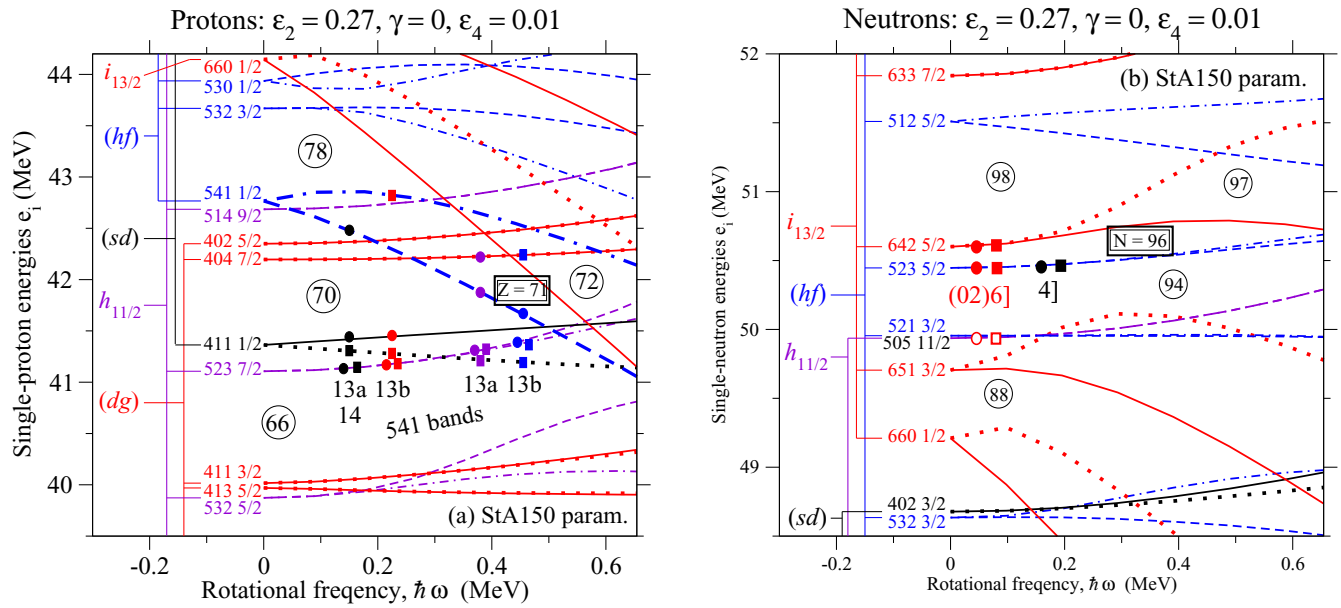

FIG. 3. Single-routhian orbitals at an average deformation calculated for the normal-deformed bands in ^{167}Lu, $(\varepsilon_2, \gamma, \varepsilon_4) \approx (0.27, 0^\circ, 0.01)$ for (a) protons and (b) neutrons. Dashed lines are used for negative parity orbitals while dots are used for signature $\alpha = -1/2$. It is indicated how the proton orbitals can be classified as dg ($d_{5/2}g_{7/2}$), sd ($s_{1/2}d_{3/2}$), $h_{11/2}$ and hf ($h_{9/2}f_{7/2}$), where it is not always possible to distinguish between the low-j $\mathcal{N} = 4$ dg and sd orbitals. The neutron orbitals are classified as hf ($h_{9/2}f_{7/2}$), $i_{13/2}$, and $h_{11/2}$. The filling of the orbitals above the $Z = 66$ and $N = 94$ gaps according to our interpretation is illustrated for the 541 bands where circles are used for signature $\alpha = 1/2$ and squares for $\alpha = -1/2$. At low spin for the 13a and 13b configurations, the proton configurations illustrated at low frequencies are combined with the '(02)6]' neutron configuration while at high spin, the proton configurations illustrated at high frequencies are combined with the '4]' neutron configuration. Band 14 is built from the proton configuration to the left combined with the '4]' neutron configuration.

Branching ratios for transitions between bands 1 and 10 are also calculated in the present two-band mixing model, assuming the same transition strengths, B(E2)'s, within the smooth unperturbed bands and no transition probabilities connecting these bands. These calculations show a reasonable agreement with experiment in that the observed bands follow the strongest calculated branching ratios; see Fig. 2(a) [Fig. 2(b)] for $\alpha = -1/2$ ($\alpha = 1/2$) bands. Red numbers show the experimental relative intensities while the calculated branching between in-band and out-of-band transitions are shown in percentage by black numbers. For the $\alpha = -1/2$ bands in Fig. 2(a), the connecting transitions with a calculated branching ratio of 22% and 8% at $I = 29.5$ between the two bands are observed. However, a transition with a calculated 16% branching ratio from the $I = 31.5$ state of band 10 to the $I = 29.5$ of band 1 is not seen in the experiment. For $\alpha = 1/2$ in Fig. 2(b), the connecting transitions with a predicted 38% and 22% branching ratio are observed whilst the one with a predicted 6% branch is not observed.

Band 9a and the band which is assigned as TSD1, band 11, interact at $I \approx 30$ in a similar way as bands 1 and 10; see Fig. 2(b). Band mixing calculations were performed also for these bands in the spin range $I = 26.5$–36.5. With the moment of inertia parameterized with a linear dependence on I, it was possible to reproduce all observed states in the studied spin range within ± 10 keV, using an interaction matrix element of 24 keV. As seen in Fig. 2(b), the band mixing calculation predicts a transition with a 22% branching ratio from the $I = 32.5$ state of band 11 to the $I = 30.5$ state of band 9a which is not observed while the transitions with a lower predicted branching ratio, 15%, 19%, and 8% are observed. We note that this crossing is disturbed by other bands, bands 5 and 7, which are only observed below the crossing. Therefore, the assumption of a two-band crossing is questionable in this case. It is clear that the bands interact but it is clearly more questionable if the two bands "cross" and exchange character around $I = 30$. Thus, in our interpretation below, we will not treat these bands as crossing. Furthermore, we will not try to interpret band 11 (the TSD band) which has been discussed in Ref. [44].

B. Bands based on $\mathcal{N} = 4$ band heads

In the previous section, the crossing between bands 1 and 10 at $I \approx 30$ was analyzed. It is now instructive to analyze the positive one-quasiparticle bands in some more detail, i.e., the bands based on band heads with the odd proton in a positive parity orbital. As seen from the single-routhian orbitals in Fig. 3 there are three such orbitals close to the Fermi surface, the [404]7/2 and [402]5/2 orbitals of $d_{5/2}g_{7/2}$ (dg) origin and the [411] 1/2 orbital of $s_{1/2}d_{3/2}$ (sd) origin. The experimental bands based on these band heads are drawn in Fig. 4. As can be concluded, e.g., from Fig. 3 in Ref. [13] it is evident which states should be assigned to the different band heads at low spin. Furthermore, the lowest band, starting on the [404]7/2 band head, remains separate from the other bands up to the crossing at $I \approx 30$, i.e., it must be assigned as [404]7/2 in this full spin range. In general, the [404]7/2 and [402]5/2

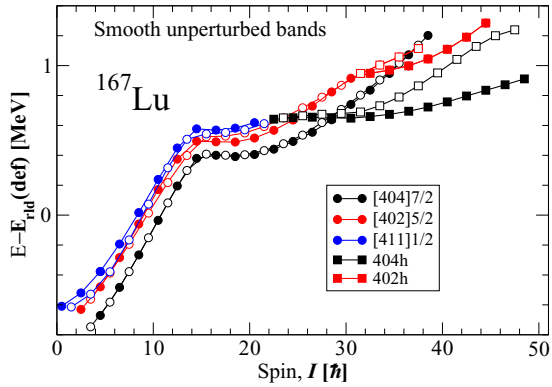

FIG. 4. Experimental bands built on the $\mathcal{N} = 4$ proton band heads which will be compared with CNS and CNSB calculations.

Nilsson orbitals have very similar properties because they have both $n_z = 0$; i.e., they have all quanta in the perpendicular direction. Furthermore, because they have relatively high spin values along the symmetry axis, $\Omega = 7/2$ and $5/2$, respectively, they will only give a small spin contribution as seen from the small slopes in Fig. 3, where we can also see that the two signatures remain degenerate up to the highest frequencies shown in the figure. Thus, the band which follows the same trend as the [404]7/2 band but ≈200 keV excited in energy must be assigned as [402]5/2. This is in contradiction to the band assignment according to Ref. [13]. This difference is understood from the fact the $\frac{11}{2}^-$ states of the [402]5/2 and [411]1/2 bands are almost degenerate and it is unclear how the bands should be connected. Compared with Ref. [13], we have thus formed a band-crossing at $I = 11/2$. The way we have formed bands is thus mainly based on the energies. $M1$ transitions are observed both within the bands and connecting the bands indicating that these bands are strongly mixed. In any case, for a general understanding of the bands within our cranking formalism, the labeling in Fig. 4 is certainly preferable. This means that comparing with Fig. 1, we can conclude that

(i) Band [404]7/2 is composed of band 1 up to $I \approx 30$ and then by band 10.
(ii) Band [402]5/2 in the spin range $I \approx 5.5$–30 is composed by bands 9a and 8b, see Fig. 1.
(iii) Band [411]1/2 in the spin range $I \approx 5.5$–21.5 is composed of 8a and 9b
(iv) The band which we label 404h (where h refers to "high spin") is composed of band 10 in the spin range $I \approx 22.5$–30 and from band 1 for spin values above $I \approx 30$.
(v) Band 402h is built from band 9a and 8b above $I \approx 30$

III. CNS AND CNSB CALCULATIONS

A. Formalism

In the cranked Nilsson-Strutinsky (CNS) model [7,9,18] the Hamiltonian is taken as

$$H = H_{\rm MO}(\varepsilon_2, \gamma, \varepsilon_4) - \omega j_x, \qquad (1)$$

TABLE I. StA150 κ and μ parameters for $\mathcal{N} = 4$, 5, and 6 proton and neutron shells. These parameters are an arithmetic average of the standard and $A = 150$ parameters where it is only the values written in bold which are different in the two sets.

	κ_p	μ_p	κ_n	μ_n
$\mathcal{N} = 4$	**0.0675**	**0.5337**	0.07000	0.3900
$\mathcal{N} = 5$	0.0600	**0.6000**	0.06200	0.4300
$\mathcal{N} = 6$	0.0540	0.6000	0.06200	**0.3700**

where $H_{\rm MO}$ denotes the modified oscillator Hamiltonian [46] and ωj_x is the cranking term. The renormalized total energies are calculated as the sum of the rotating liquid-drop energy and the shell energy using the Strutinsky method [47]. The Lublin-Strasbourg drop (LSD) model [48] is used for the static liquid drop energy while a radius parameter $r_0 = 1.16$ fm and a diffuseness parameter $a = 0.6$ fm is used for the rigid body moment of inertia [9].

In addition to the unpaired CNS calculations, we have also carried out calculations in the cranked Nilsson-Strutinsky-Bogoliubov (CNSB) formalism with pairing included [23,24]. The CNSB model is based on the ultimate cranker formalism [10,11], using the same modified oscillator potential as the CNS model, plus a monopole pairing term. The Hamiltonian for either protons or neutrons can be written as

$$H = H_{\rm MO}(\varepsilon_2, \gamma, \varepsilon_4) - \omega j_x + \Delta(P^\dagger + P) - \lambda \hat{N}, \qquad (2)$$

where $P^\dagger$ (P) and $\hat{N}$ are the pair creation (annihilation) and particle number operators, respectively. In this approach, the microscopic energy after particle number projection, is minimized in a mesh of the pairing parameters, Fermi energy λ_p and λ_n, and pairing gap Δ_p and Δ_n, as well as in the deformation space. As seen in Eqs. (1) and (2), the CNS and CNSB Hamiltonians are different only in the pairing terms. Both CNS and CNSB calculations are carried out in a quadrupole and hexadecapole deformation mesh $(\varepsilon_2, \gamma, \varepsilon_4)$ with the same κ and μ parameters.

For the κ and μ Nilsson model parameters, we have used the set StA150 [49] which is the average of $A = 150$ [11] and standard [7] κ and μ' parameters. This is motivated by the fact that the $A = 150$ parameters have been fitted for nuclei with $N \approx 90$, and standard parameters are more appropriate for the well deformed nuclei in the middle of the rare-earth region, where the nucleus ^{167}Lu with $Z = 71$ and $N = 96$ is somewhere between these two regions. The StA150 parameters are listed in Table I for the shells where the two sets are not identical, $\mathcal{N} = 4$, 5, and 6.

The only preserved quantum numbers in the CNSB formalism are parity π and signature α for protons and neutrons; i.e., the configurations can be labeled as $(\pi_p, \alpha_p)(\pi_n, \alpha_n)$. The advantage of the CNS calculations is mainly that configurations can be fixed in a much more detailed way. Thus, the diagonalization is carried out in a rotating harmonic oscillator basis [7] where the small couplings between the $\mathcal{N}_{\rm rot}$-shells are neglected making $\mathcal{N}_{\rm rot}$ a preserved quantum number. Furthermore, within the $\mathcal{N}_{\rm rot}$-shells, it is possible to define approximate quantum numbers where it is generally

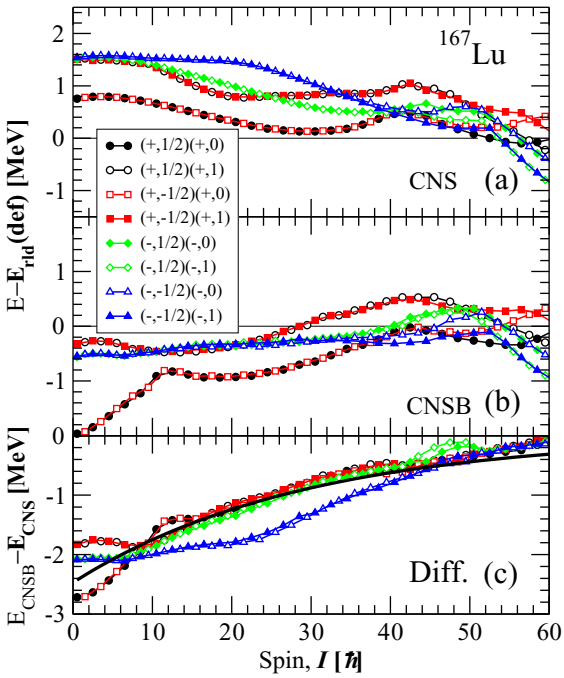

FIG. 5. Calculated unpaired (a) and paired (b) yrast bands and their differences (c) in ^{167}Lu for the positive parity configurations. The average pairing energy is shown by a black line in panel (c).

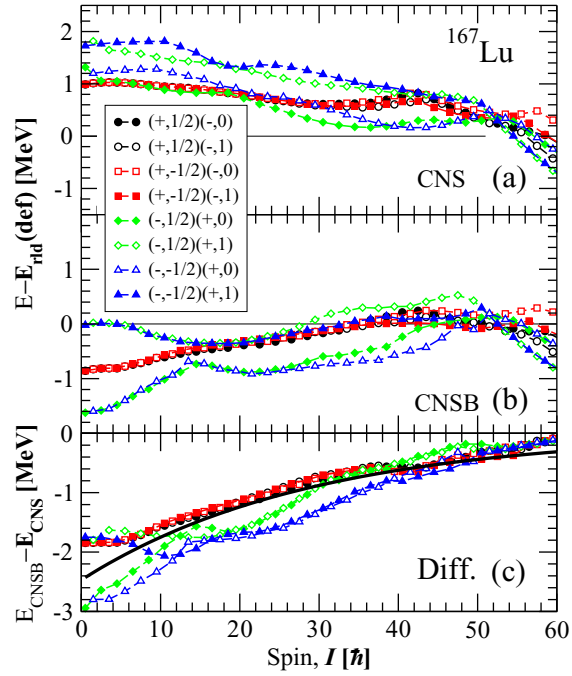

FIG. 6. Same as described in the caption of Fig. 5 but for negative parity configurations.

straightforward to distinguish between orbitals with their major amplitude, either in the intruder high-j shell or in the other "low-j" shells. Indeed, sometimes a further distinction specifying orbitals as belonging to pseudo-spin partner orbitals is also possible; see Fig. 3(a). Here, we will mainly make a distinction between high-j and low-j which means that configurations in ^{167}Lu can be labeled as $[p_1(p_2p_3); (n_1n_2)n_3]$, where p_1 represents the number of $h_{11/2}$ protons and n_3 the number of $i_{13/2}$ neutrons. The labels p_2 and p_3, represent the number of protons of $f_{7/2}h_{9/2}$ and $i_{13/2}$ character while n_1 and n_2 are the number of neutron holes in $\mathcal{N} = 4$ and $h_{11/2}$ orbitals, respectively. These numbers in parentheses are specified only if nonzero. For ^{167}Lu with 71 protons and 96 neutrons, configurations can be written in full as

$$\pi(\mathcal{N}=4)^{-(p_1+p_2+p_3-1)}(h_{11/2})^{p_1}(f_{7/2}h_{9/2})^{p_2}(i_{13/2})^{p_3},$$
$$\nu(\mathcal{N}=4)^{-n_1}(h_{11/2})^{-n_2}(f_{7/2}h_{9/2})^{14+n_1+n_2-n_3}(i_{13/2})^{n_3},$$

relative to a $Z = 70$ proton core with all shells up to $\mathcal{N} = 4$ filled and a neutron core with all j shells up to neutron number $N = 82$ filled.

The transitional quadrupole moment Q_t is calculated from the deformation of a state, where the formula is given, e.g., in Refs. [50,51].

B. Comparison of CNS and CNSB calculations

The comparison of the 16 CNS and CNSB yrast combinations designated with $(\pi_p, \alpha_p)(\pi_n, \alpha_n)$ is shown in the full spin range, $I = 0$–60, in Figs. 5 and 6 for the positive and negative parity configurations, respectively.

The energy differences between the unpaired and paired calculations, which correspond to the pairing correction energies for the yrast configurations, are displayed in Figs. 5(c) and 6(c). The band crossing (backbending) in the paired CNSB yrast bands with the $(+, 0)$ neutron configuration is evident. It is well-known that the rotational alignment of one $i_{13/2}$ neutron pair is responsible for this band crossing, which is usually seen in the rotational bands in the rare-earth nuclei in the spin region $I = 12$–16 [52].

One can also see a clear trend for the pairing correction energies in different configurations of ^{167}Lu. At higher spins than $I \approx 20$, there are no significant discontinuities in the differences between the CNSB and CNS yrast lines in ^{167}Lu. It suggests that the calculated crossings at higher spin than $I \approx 20$ are similar in two formalisms. It indicates that these band crossings can be understood as caused by crossings between unpaired CNS configurations.

In Figs. 5 and 6, the configurations with negative parity for the protons have a stronger pairing in the $I \approx 10$–40 spin range than the other configurations. This is especially true for the $(\pi, \alpha)_p = (-, -1/2)$ configurations but to some extent also for $(\pi, \alpha)_p = (-, 1/2)$. It appears that the reason is that the orbital which is blocked in these configurations is far away from the Fermi surface; see Fig. 3(a). Thus, at low frequencies, the [523]7/2 orbital is far below the Fermi surface while the [514]9/2 orbital is far above. At the deformation used in Fig. 3, it is only for somewhat higher frequencies that the $\alpha = 1/2$, [541]1/2 orbital will come in the Fermi energy region. The blocking of an orbital close to the Fermi energy will reduce the pairing correlations while blocking of an orbital further away will have a smaller effect. Thus, the calculated pairing energies in the different configurations

are consistent with expectations based on the position of the orbitals around the Fermi energy.

To get a more realistic results from the CNS calculations, we fit a smooth function to the curves in Figs. 5(c) and 6(c), corresponding to the average pairing correction energy. Then it is straightforward to add this average pairing correction to the CNS results. A least square fit of an exponential function in the $I = 0$–60 region of spin results in

$$E_{\text{pair}} = -2.47\exp(-I/29).$$

In the calculations presented below, this average pairing energy will be added to the CNS energies.

C. Expected low-lying configurations

The routhians for protons and neutrons presented in Fig. 3 can be used to get a general understanding of which configurations are expected to be observed in ^{167}Lu. The proton diagram suggests that at low spin for positive parity, the proton valence space configurations will have the odd proton in the [404]7/2 or [402]5/2 orbitals which are pseudospin partners in the $d_{5/2}g_{7/2}$ (dg) shells. Also the [411]1/2 orbital of $s_{1/2}d_{3/2}$ (sd) origin comes rather close to the Fermi energy. For negative parity, the $h_{11/2}$ orbitals [523]7/2 and [514]9/2 are found at a similar distance from the Fermi energy. It is clear that also the [541]1/2 orbital of $h_{9/2}f_{7/2}$ (hf) origin could be competitive. For higher frequency, this hf orbital and also the $i_{13/2}$ [660]1/2 orbital comes close to the Fermi energy, where the down-slope of the routhians shows that these orbitals will give a significant spin contribution.

Because of pairing, the favored low-spin band heads will be formed when the proton valence space configurations are combined with an even parity neutron configuration. The resulting *one-quasiparticle configurations* will be dominated by $\nu(i_{13/2})^4$ as can be concluded from Fig. 3(b). However, this figure suggests that also the $(i_{13/2})^5$ configurations with an odd neutron in the $i_{13/2}$ as well as in the hf orbitals will come low in energy. When they are combined with the proton valence space configurations, *three-quasiparticle configurations* are formed. They will become competitive in energy around $I =$ 10–15, because after the first backbend, also the $\nu(i_{13/2})^4$ configurations will have three "odd particles"; i.e., they will have a similar pairing energy as the three-quasiparticle configurations. It is then our experience that for higher spin values, the spin is mainly built from the gradual alignment of the valence particles and it is not meaningful to describe them as having a fixed number of quasiparticles.

The main features of the level scheme can be understood from the discussion above. However, it is also possible to read out some additional features from Fig. 3. Thus, the neutron [505]11/2 orbital of $h_{11/2}$ origin comes close to the Fermi surface, which means that configurations with one or two holes in this orbital might become competitive. It appears that no configurations with one hole is observed in ^{167}Lu, while for configurations with two holes, it is clear that 6 $i_{13/2}$ orbitals will be occupied; see Fig. 3(b). Note, however, that the sixth $i_{13/2}$ orbital with signature $\alpha = -1/2$ goes away from the Fermi energy with increasing spin. Thus, it is only for low spin values that $\nu(h_{11/2})^{-2}(i_{13/2})^6$ configurations are competitive in energy. Furthermore, with no $h_{11/2}$ holes, for $(i_{13/2})^5$ configurations it is only those with the 5th neutron in the signature $\alpha = 1/2$ branch which are competitive in energy, while $(i_{13/2})^6$ configurations will come too high in energy to be of practical interest. The conclusion is thus that there are only four neutron configurations of interest, namely, $(i_{13/2})^4$, $(i_{13/2})^5$ with two signatures for the hf neutron and $(h_{11/2})^{-2}(i_{13/2})^6$. Note the signature degeneracy for the [523]5/2 orbital in Fig. 3(b); i.e., signature degenerate bands are expected in the $(i_{13/2})^5$ configurations.

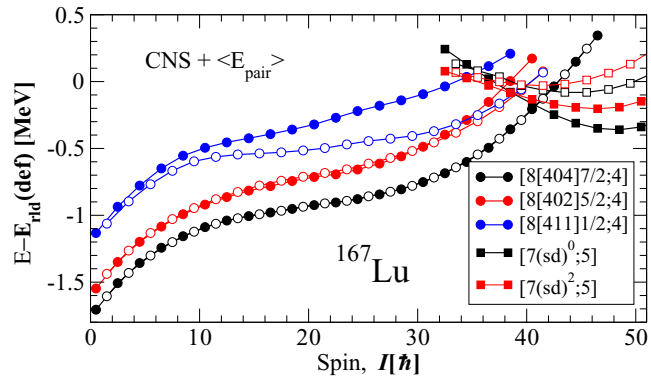

FIG. 7. CNS configurations which are assigned to the experimental bands in Fig. 4.

IV. INTERPRETATION OF THE BANDS

In our analysis of the observed bands, we will first consider those which start out as one-quasiparticle bands, namely, those which are built on $\mathcal{N} = 4$ orbitals in Sec. IV A, those built on $h_{11/2}$ orbitals in Sec. IV B and those based on the [541]1/2 orbital of hf origin in Sec. IV C. For the latter band, which is yrast at low spin, we will conclude that up to $I \approx 20$, it is based on a configuration with two $h_{11/2}$ neutron holes. Then in Sec. IV D, we will consider the bands of both parities which are assigned to start out as three-quasiparticle bands. We may note that one of the three-quasiparticle bands is only seen at high spin and because it feeds into the $\mathcal{N} = 4$ bands, it will be treated in Sec. IV A.

A. Bands based on the $\mathcal{N} = 4$ band heads

The observed bands based on the proton $\mathcal{N} = 4$ orbitals are shown in Fig. 4. The configurations calculated in CNS which are assigned to these bands are drawn in Fig. 7. The observed and calculated bands show the same structure with the [404]7/2 band as yrast and then [402]5/2 and [411]1/2 as the first and second excited bands. The observed bands for spins up to $I \approx 30$ are only spread within 300 keV while the calculated ones are somewhat more spread, i.e., within 600–700 keV. This is, however, a rather small difference and it would only require a small change of the single-particle parameters to put the [411]1/2 orbital closer to the Fermi energy; see Fig. 3(a). All the observed bands go through a backbend at $I \approx 14$ which is of course the AB crossing where two $i_{13/2}$ neutrons align. Then, at $I \approx 30$, band crossings are observed both in the [404]7/2 and [402]5/2 bands. In

Ref. [13], it is suggested that this crossing in the [404]7/2 band is caused by another alignment among the $i_{13/2}$ neutrons, the CD crossing. The idea is thus that the lowest energy band, labeled 404h, has four $i_{13/2}$ neutrons aligned while the upper band has only two such neutrons aligned. Our experience is that, if such configurations could be formed, then the band with only two neutrons aligned would be very unfavored in energy and it seems very strange that this band can be followed for approximately 10 units of angular momentum up to $I \approx 40$, where this higher band is only about 200 and 400 keV above the two signatures of the bands with four $i_{13/2}$ neutrons aligned. Even more strange is, however, that the yrast band shows an appreciable signature splitting while the excited band does not. Because in the full spin range, the odd particle will be in the signature degenerate [404]7/2 orbital, see Fig. 3(a), no such splitting is expected as also noted in Ref. [13]. Furthermore, the calculations including pairing which are presented below do not show any more crossing after the AB crossing. Our interpretation is then that after the first AB crossing, the pairing energy is severely quenched so that no CD crossing is observed; instead the remaining alignment among the $i_{13/2}$ neutrons occurs gradually as described by the unpaired CNS calculations.

1. Interpretation of the band crossing at $I \approx 30$

The question is then how the band labeled 404h which intersects the [404]7/2 band at $I \approx 30$ should be understood. From the single-routhian diagrams in Fig. 3 one could expect a band where one [523]7/2 proton is lifted to the [541]1/2 orbital. The corresponding band labeled [7(10);4], not shown in Fig. 7, will cross the lowest [8;4] band somewhat above $I = 40$. However, this band will have the odd proton in the [404]7/2 orbital which means that two signature degenerate bands would be expected contrary to experiment. Indeed, another band with negative parity for both protons and neutrons, $\pi(h_{11/2})^7\nu(i_{13/2})^5$ or [7;5] will cross the lowest [8;4] band, the [404]7/2 band, at a slightly lower spin value around $I = 40$, see Fig. 7. Note that with this interpretation for the 404h band, its signature splitting is about the same as in the calculated band assigned to it, the [7;5] band. The signature splitting is caused by the odd hf neutron with the odd $h_{11/2}$ proton in its favored signature. An alternative would be to leave the hf neutron in the favored signature and form the two signatures from the odd $h_{11/2}$ orbital instead. However, the unfavored signature branch would then come at a higher energy and the signature splitting would be considerably larger in calculations than in experiment; see Fig. 17 below.

It is seen in Fig. 4 that there is a similar crossing in band [402]5/2 as in band [404]7/2, also at spin $I \approx 30$ which suggests a similar structure change in the two bands. Indeed, as becomes evident from Fig. 3(a), with 7 protons in the $h_{11/2}$ shell, the $\mathcal{N} = 4$ protons can have different distributions over the sd and dg orbitals. Note also that the calculated deformation at $I \approx 40$ for the [7;5] configuration is $\varepsilon_2 \approx 0.22$ where the sd orbital, [411]1/2, and the dg orbitals, [404]7/2 and [402]5/2, come much closer in energy than at the deformation in Fig. 3, $\varepsilon_2 = 0.27$.

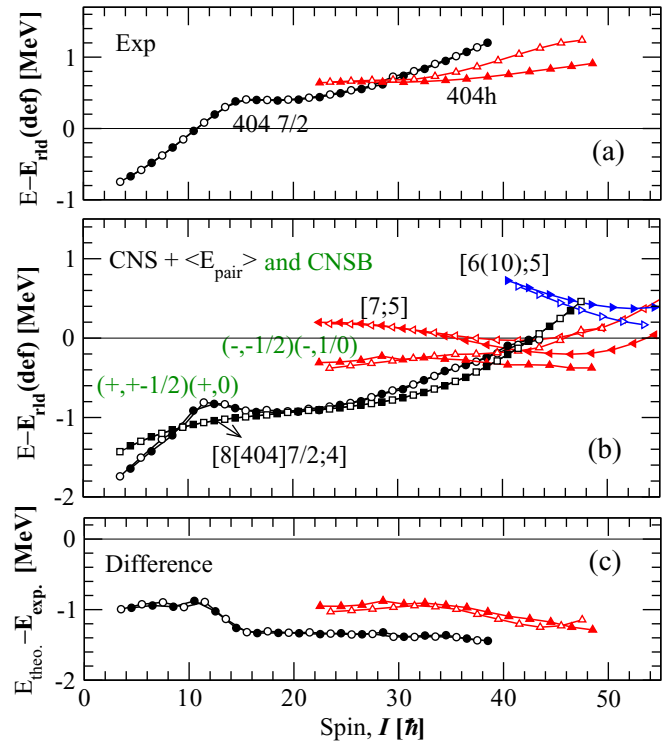

FIG. 8. Experimental energies (a) and theoretical "CNS + average pairing" and CNSB energies (b) relative to a rotating liquid drop and the differences between the experiment and the CNSB yrast configurations (c) as a function of spin for $\mathcal{N} = 4$ configurations.

It turns out that with constraints on the distribution of protons in the dg and sd orbitals, respectively, those with a closed $Z = 64$ core, $(sd)^0$ and those with two (dg) holes in the core, i.e., two (sd) protons, $(sd)^2$, have a very similar energy; see Fig. 7. However, these two configurations have a different deformation, $\gamma \approx -30^\circ$ and $\gamma \approx -10^\circ$, which means that the division into (sd) and (dg) orbitals is not so well-defined. In general, such a division appears to be pretty straightforward for positive values of γ and $\gamma \approx 0$ but more arbitrary for large negative values of γ where the two highest dg orbitals and the lowest sd orbital are more strongly mixed. Thus, the energy difference between the $(sd)^0$ and $(sd)^2$ bands in Fig. 7 is uncertain but these calculations show that there is room for two [7;5] bands to explain the observed 404h and 402h bands.

A problem is that the crossings are observed at $I \approx 30$ while, they are calculated at $I \approx 40$. However, as noted below, with pairing included the calculated crossing will come at a lower spin value closer to experiment.

2. CNSB calculations

It is only for the bands which are yrast in the groups with parity and signature fixed for protons and neutrons that it is straightforward to compare with paired calculations. Thus, for the bands which are lowest in energy in Figs. 4 and 7, such a comparison is provided in Fig. 8. In this figure, the observed bands are shown relative to the rotating liquid drop energy in the upper panel, the corresponding calculated bands in CNS with average pairing and CNSB are shown in the middle panel

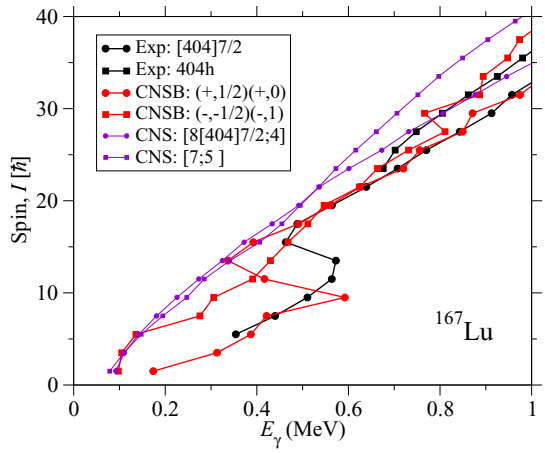

FIG. 9. Spin I versus transition energy E_γ for the $\alpha = 1/2$ branches of the observed bands [404]7/2 and 404h are compared with calculations for the configurations assigned to these bands in the CNS and CNSB formalisms.

with the difference between experiment and CNSB calculations in the lower panel. Comparing the two calculations in the middle panel, it turns out that the CNSB pairing will be stronger than the average for the [7;5] bands while, for $I = 30-40$, it will be weaker than the average in the [8;4] bands. Consequently, relative to CNS with average pairing, the crossing between the two bands will come at a lower spin in CNSB and thus closer to experiment. Furthermore, the two difference curves in the lower panel comes relatively close together, separated by approximately 400 keV which is clearly within the general uncertainty of the calculations. Thus, from relative energies and also from the signature splitting, the description of this crossing at the yrast line is well described as a crossing between an [8;4] and a [7;5] configuration. Concerning the interaction strength between these two rather different configurations, it is somewhat more difficult to judge if the observed value around 30 keV, see Sec. II A, is what would be expected.

3. Alignments

The alignment of the observed $\alpha = 1/2$ branches of bands 1 and 10 is discussed in the Appendix. When we let these bands cross at $I \approx 30$, they are referred to as bands [404]7/2 and 404h; see Fig. 4. Their spin values are drawn versus the transition energy in Fig. 9. The first AB crossing in the [404]7/2 band has been studied in detail previously; see, e.g., Ref. [53]. It is, however, satisfying to observe that it is well explained in the present CNSB calculations while this paired crossing is of course not reproduced in the CNS calculations. Our main interest here is, however, the spin difference between the [404]7/2 and the 404h bands when they cross around $I \approx 30$, where the observed value is around $2.5\hbar$ as determined in the Appendix and which can also be read out from Fig. 9. It is then very satisfying, that the CNSB alignments reproduce the experimental values for both bands in an extended frequency range, and thus also their difference, on the average. The rather large fluctuations in the calculated values can probably be explained by the fact that we do not interpolate in the pairing space; i.e., the energy is taken as the lowest value in the (Δ, λ) mesh.

The values calculated in the CNS formalism are also drawn in Fig. 9. It is interesting that also at high spin, $I = 30$–$40\hbar$, the values calculated in CNS and CNSB are rather different. If an average pairing is added, then the CNS results will of course come closer to CNSB (and experiment). However, for example, the spin difference between the [8;4] and [7;5] configurations is still clearly larger than for the corresponding CNSB configurations and thus also more different from experiment. This appears consistent with the observation from Fig. 8 that the different pairing for the [8;4] and [7;5] configurations is important to get a satisfactory agreement between experiment and calculations.

4. Higher spin discontinuities

In the unfavored signature of the observed 404h band at the highest spin, a small disturbance is seen suggesting an interaction or crossing with some other bands. Indeed, different bands come down at high spin, for example, with one proton excited to [541]1/2 as shown in Fig. 8(b) and at a similar energy, bands with a proton excited to the [660]1/2 orbital [not shown in Fig. 8(b)]. We may note, however, that the crossing between the $\alpha = -1/2$ [7;5] and [6(10];5] bands in Fig. 8(b) does not only correspond to lifting a proton from the [523]7/2 to the [541]1/2 orbital but also to a signature change not only for this proton but also for the negative parity neutron. Furthermore, while it is difficult to identify any disturbance of the $\alpha = 1/2$ [7;5] band from Fig. 8 such a disturbance is seen in the relative alignment plots in Fig. 19; i.e., this plot suggests a similar disturbance in both signatures of the [7;5] band. Indeed, a closer look on the [7;5] bands reveals a shape change from $\gamma \approx 0$ to γ approaching -30° in both signatures of the [7;5] band. This shape change is clearly related to the different shapes of the two [7;5] bands, $(sd)^0$ and $(sd)^2$, discussed above. The effect on the energies from this shape change is seen rather clearly at $I \approx 46$ in the $\alpha = -1/2$ but not in the $\alpha = 1/2$ branch of the calculated [7;5] band in Fig. 8. Thus, our interpretation is that this shape change causes the small discontinuity observed at $I \approx 46$ in the 404h band drawn in Fig. 8(a).

5. Bands 6 and 7

Band 7 decays to the [404]7/2 band with two rather intense transitions, $14.5 \rightarrow 12.5$ and $16.5 \rightarrow 14.5$. In addition, a weak transition is observed to band 4, $26.5 \rightarrow 24.5$, which can be understood because especially the $I = 24.5$ states of bands 7 and 4 come close together. The transitions to the [404]7/2 band suggests some relation with this band and the energy curve of band 7 suggests that it can be understood as a continuation of the [404]7/2 band with no AB alignment. This might suggest that the crossing seen in band 7 at $\hbar\omega \approx 0.32$ MeV can be understood as a BC alignment. The energy curve of band 6 and its decay to the [402]5/2 $\alpha = -1/2$ band suggests a similar scenario for this band, namely, that it could be the $\alpha = -1/2$ continuation of the [402]5/2 band with no AB alignment. However, the fact that no BC crossing is seen

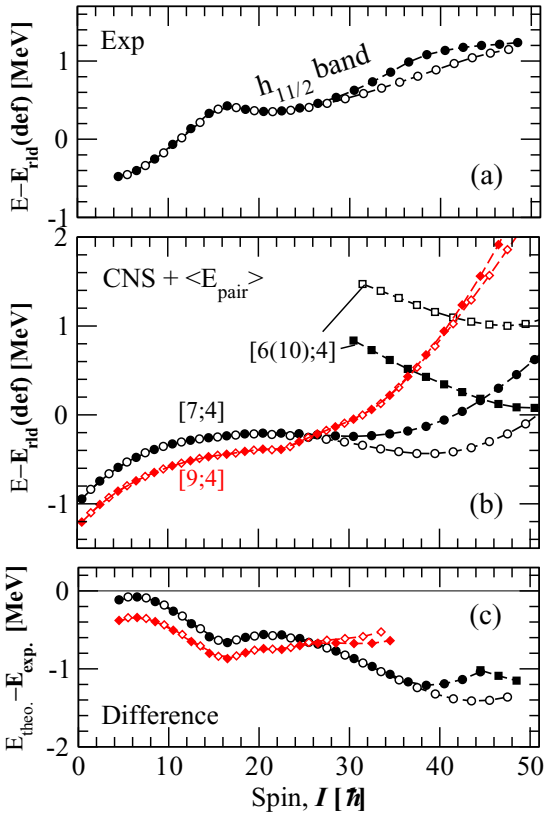

FIG. 10. Experimental energies (a) and theoretical "CNS + average pairing" energies (b) relative to a rotating liquid drop and their differences (c) as a function of spin for the $h_{11/2}$ band in ^{167}Lu.

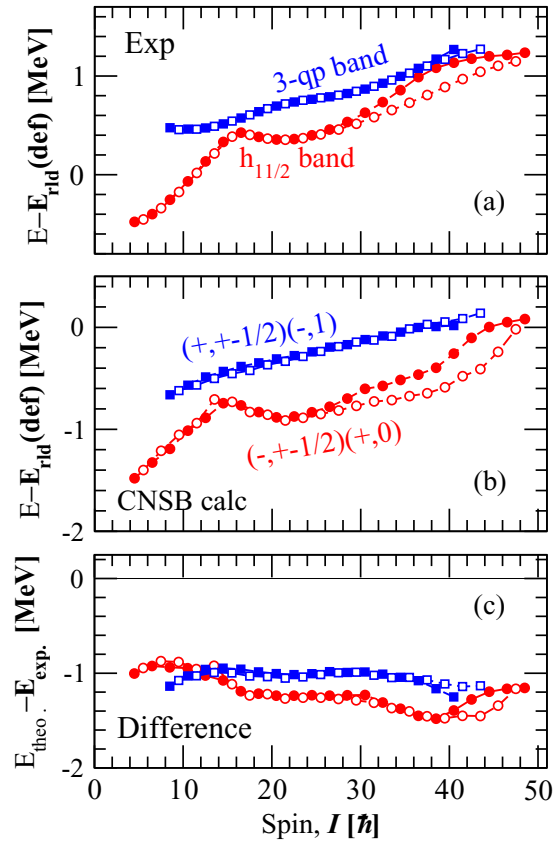

FIG. 11. Experimental energies (a) and theoretical CNSB energies (b) relative to a rotating liquid drop and their differences (c) as a function of spin for the $h_{11/2}$ band (Sec. IV B) and the three-quasiparticle band 2 (Sec. IV D) in ^{167}Lu.

and the fact that band 6 has several links to a negative parity 541 band makes the interpretation very tentative.

B. The $h_{11/2}$ band (band 15)

The signature partner $h_{11/2}$ bands (Bands 15 in Ref. [13]) are the lowest negative-parity bands in ^{167}Lu for spin values above $I \approx 18$. The CNS configurations with either 7 or 9 $h_{11/2}$ protons, [7;4] or [9;4] and thus with the odd proton in either [523]7/2 or [514]9/2 come at a very similar energy at low and intermediate spin; see Fig. 10. Thus, at low spin, it is somewhat uncertain if the $h_{11/2}$ band should be assigned to one or the other of these two bands or maybe rather a mixture of them. At higher spin values, the [7;4] configuration is clearly favored in energy and also the signature splitting is consistent with the [7;4] interpretation. Thus, because no discontinuity is seen in the observed band in the $I \approx 16-40$ spin range, it appears well established that above the backbend at $I \approx 16$, where pairing is severely quenched, the $h_{11/2}$ band should be assigned to the [7;4] configuration, i.e., with the odd proton in the [523]7/2 orbital. This is contrary to Ref. [13], where the $h_{11/2}$ band is assigned to a configuration with the odd proton in the [514]9/2 orbital.

Our calculations suggest that the observed crossing in the $\alpha = 1/2$, $h_{11/2}$ band at $I \approx 40$ is caused by the excitation of a proton from [523]7/2 $h_{11/2}$ orbital to the [541]1/2 $h_{9/2}$ orbital at the frequency $\hbar\omega = 0.5$ MeV where these orbitals cross; see Fig. 3(a). The observed crossing in the $h_{11/2}$ band is thus explained as a crossing between the $\alpha = 1/2$ [7;4] and [6(10);4] configurations in the CNS labeling. A similar crossing is observed in ^{168}Hf [34,38]. Our interpretation is in agreement with Ref. [13] where this crossing is labeled as an fg crossing. Note that no corresponding crossing is expected for signature $\alpha = -1/2$. This is understood from the high energy of the $\alpha = -1/2$ [541]1/2 orbital in Fig. 3(a) corresponding to a high energy of the corresponding [6(10);4] band, see middle panel of Fig. 10.

Considering the one-quasiparticle configurations with negative parity, $(-, \pm 1/2)(+, 0)$, those with the odd proton in the [541]1/2 orbital of hf origin are generally lower in energy than those with an odd $h_{11/2}$ proton in the CNS calculations. However, as noted in Sec. III B, pairing is stronger in the "$h_{11/2}$ configurations". Therefore, in the CNSB calculations, the $(-, \pm 1/2)(+, 0)$ yrast configurations have in general the odd particle in $h_{11/2}$. Thus, the observed $h_{11/2}$ band can be compared with the full pairing CNSB configurations as done in Fig. 11. The difference between experiment and calculations is now more constant at a value around or just below -1 MeV. As would be expected, it is especially below the first $i_{13/2}$ band-crossing where the average pairing energy comes out too small.

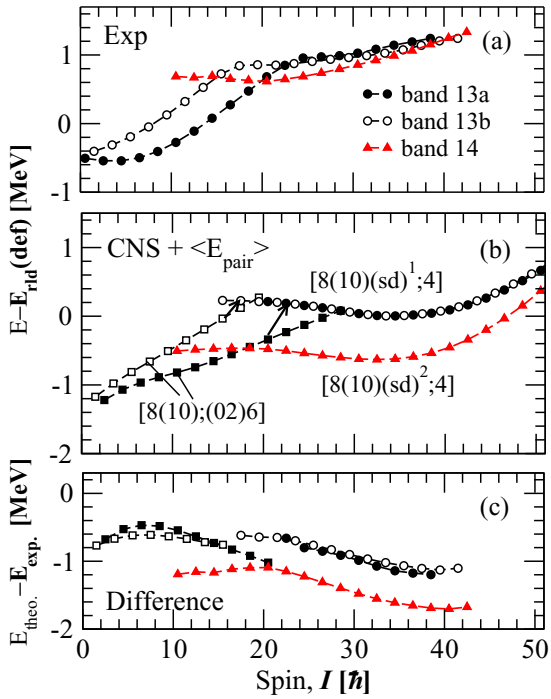

FIG. 12. Experimental energies (a) and theoretical "CNS + average pairing" energies (b) relative to a rotating liquid drop and their differences (c) as a function of spin for the 541 bands in ^{167}Lu, i.e., the bands 13a, 13b, and 14.

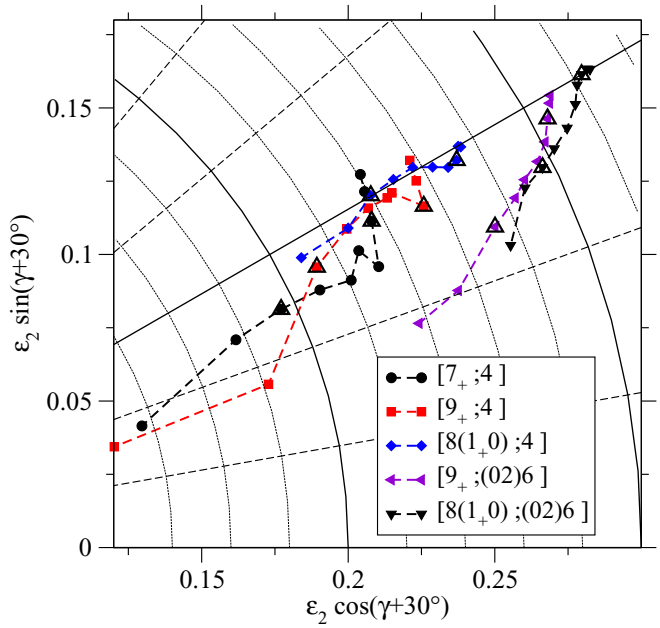

FIG. 13. Deformation trajectories calculated in the CNS formalism for some negative parity configurations in ^{167}Lu, drawn to illustrate the polarization effects of a [541]1/2 proton and two $h_{11/2}$ neutron holes. The trajectories are drawn in steps of $6\hbar$ in the spin range $I = 4.5$–58.5. The deformation within these fixed configurations will decrease with increasing spin where the points for $I = 16.5$ and 46.5 are highlighted by big triangles. In the legend, the subscript "+" specifies the signature for the odd proton, $\alpha = 1/2$.

When checking the CNSB calculations in more detail, it turns out that for signature $\alpha = 1/2$, the [541]1/2 band might come slightly below the $h_{11/2}$ band for some spin values. However, because the two bands have a very similar energy in these cases, the error which is introduced because the odd proton is placed in the "wrong orbital" is so small that it is not noticeable in Fig. 11. Note also that for signature $\alpha = -1/2$, the $h_{11/2}$ band is clearly calculated lowest in energy. Therefore, the fact that the two signatures are degenerate in an extended spin range in Fig. 11 shows that also the branch with signature $\alpha = 1/2$ is in general built with an odd $h_{11/2}$ proton. The competition between the hf and $h_{11/2}$ one-quasiparticle bands will be further discussed in Sec. IV C 3 below.

C. The 541 bands (bands 13,14)

1. *The lowest 541 band in* ^{167}Lu *and neighboring nuclei*

The other low-lying one-quasiparticle negative parity configuration is built with the odd proton in the [541]1/2 orbital. It turns out that with this proton configuration, the neutron configuration with two holes in $h_{11/2}$ orbitals is favored at low spin; see Fig. 12(b). Furthermore, the low spin ranges of the 13a,b bands are well described by this $\nu(h_{11/2})^{-2}$ configuration. In the calculations, the favored $\alpha = 1/2$ signature is crossed by the corresponding configuration with no neutron holes at $I = 18$. Comparing with experiment, a very similar crossing is observed between the bands 13a and 14; i.e., this crossing is well understood in the unpaired formalism. Note, however, that also in the unpaired formalism, this corresponds to a neutron $i_{13/2}$ crossing; namely, a configuration change from $\nu(i_{13/2})^6$ to $\nu(i_{13/2})^4$ and that the $i_{13/2}$ neutrons are expected to contribute with considerably more spin in the latter than in the former configuration. In this way, this unpaired crossing has much in common with a paired $i_{13/2}$ crossing. In some sense, this is analogous to the description of the $h_{11/2}$ proton crossing in $N \approx 90$ nuclei as a crossing between configurations differing by two protons in the $h_{11/2}$ orbitals; see, e.g., Ref. [54].

It is interesting that the crossing bands 13a and 14 can be followed both before and after the crossing which is another indication that this two-level crossing can be treated in the unpaired formalism. Indeed, with moments of inertia which vary linear with spin I and with a coupling strength of 24 keV, the observed bands are fitted within ± 3 keV by two interacting smooth bands.

Rotational structures built on the proton configuration 8(10), i.e., with the odd proton in the [541]1/2 orbital, are observed systematically in the neighboring nuclei around ^{167}Lu, for example, in the isotopes ^{165}Lu [32] and ^{169}Lu [55] or the isotone ^{169}Ta [56]. The properties of such bands were discussed in Ref. [57], where the nucleus ^{165}Tm was studied in detail. In general, the backbending in [541]1/2 bands is delayed which is partly understood as caused by an increased deformation of these bands. However, the polarization effect of the [541]1/2 orbital appears to be too small as seen, for example, from measured transition quadrupole moments in the ^{165}Tm nucleus [57]. With two holes in the neutron $h_{11/2}$ orbitals the polarization effects will be much larger as seen from the calculated deformations presented in Fig. 13. The

figure shows that for one-quasiparticle configurations with the odd particle in $h_{11/2}$, the calculated quadrupole deformation at low spin values is $\varepsilon_2 = 0.24$–0.26 with an increase to $\varepsilon_2 = 0.27$–0.28 with the odd proton in the [541]1/2 orbital and then a larger increase to $\varepsilon_2 = 0.30$–0.32 with two $h_{11/2}$ neutron holes. This increased deformation might help to understand the larger crossing frequencies in the [541]1/2 bands in the $A = 160$–170 mass region. Note, however, that for ^{167}Lu, the observed crossing is rather described as caused by a crossing between "unpaired orbitals".

2. The 541 bands at higher energy

It remains to interpret the band crossings in the 13a,b bands at spin values $I \approx 22$ and $I \approx 15$, where the crossing frequencies can be read out in Fig. 17 of Ref. [13] as $\hbar\omega \approx 0.38$ and $\hbar\omega \approx 0.28$ MeV, respectively. The first idea would be that this is a standard AB crossing within the [8(10);(02)6] configuration but this appears very unlikely because then the two signatures should cross at the same frequency. Furthermore, the fact that the two signatures are essentially degenerate in energy after the crossing excludes the assumption that they are built on the two signatures of the [541]1/2 orbital because a large signature splitting is calculated for this orbital; see Fig. 3(a). Indeed, the fact that these two bands are almost as low in energy as band 14 at $I \approx 40$ makes it very unlikely that they are built with two $h_{11/2}$ neutron holes above the crossing, because such configurations are calculated to come high in energy for high spin values. Similarly, the low energy makes it very unlikely that they are built on the unfavored signature of the [541]1/2 orbital. Instead, it appears that they are both built on the favored signature of the [541]1/2 orbital. Indeed considering the proton orbitals in Fig. 3(a), we note that with the highest $\mathcal{N} = 4$ proton in the unfavored $\alpha = 1/2$ [411]1/2 orbital, this proton can be lifted to the [402]5/2 orbital as illustrated in the figure. This will lead to two close to signature degenerate bands as drawn in the middle panel of Fig. 12. With this assignment, the differences between experiment and calculations will have almost the same spin dependence at high spin for the three 541 bands drawn in Fig. 12 and with a small change of the single-particle parameters placing the [402]5/2 orbital closer to the [411]1/2 orbital, the differences would be close to overlapping. Thus, considering energies, this appears as a convincing interpretation but the fact that rather large configuration changes are required at the band-crossings of the 13a,b bands makes this interpretation somewhat questionable. However, it seems difficult to find any other more convincing interpretation of the highest spin regions of these 541 bands (bands 13a,b).

The decay of band 16 indicates some weak relation with the bands 13. Furthermore, its energy curve is similar to that of these bands. The configuration of the bands 13 at high spin is illustrated in Fig. 3, i.e., with one proton in the [404]7/2 orbital. A very tentative assignment for band 16 would then be to place this proton in the [402]5/2 orbital instead.

3. The transitional quadrupole moment, Q_t

The transitional quadrupole moment of the yrast low-spin states up to $I = 14.5$ was measured very recently [58], i.e., in the spin range where the 541 band is yrast. The experimental values are compared with the present calculations in Fig. 14. Consider first the CNS calculations, where the deformation trajectories in Fig. 13 will give a general idea about the values of Q_t in the different configurations. For our preferred configuration with two $h_{11/2}$ neutron holes, the values are much larger than the measured values, see Fig. 14. Even without these holes, the calculated values are too large.

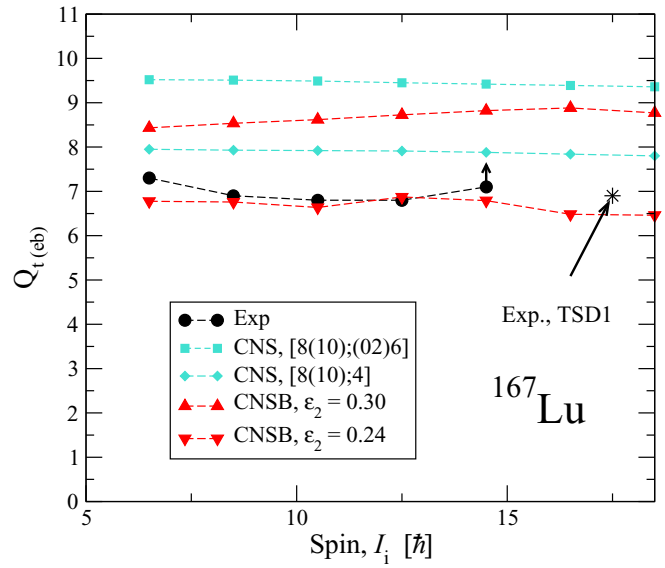

FIG. 14. The experimental transition quadrupole moments Q_t are compared with the values calculated for fixed configurations in the CNS formalism; i.e., for the configuration with an [541]1/2 proton and two $h_{11/2}$ neutron holes, [8(10);(02)6] which is our preferred assignment, and for the configuration with no neutron holes, [8(10);4]. Furthermore, the values calculated in the CNSB at the two minima of the $(-, +1/2)(+, 0)$ (see Fig. 15) are shown. Finally, the experimental value of Q_t for the TSD1 band is shown. It is obtained as an average over the most intense transitions; see Ref. [59].

To get a better understanding of the different configurations, the corresponding energy surfaces are drawn in the CNS as well as in the CNSB formalism for spin values $I = 6.5$, 10.5, and 14.5 in Fig. 15. There are two minima in these surfaces, one at $\varepsilon_2 \approx 0.30$ and the other at $\varepsilon_2 \approx 0.24$ where the former corresponds to our preferred configuration for band 13 at low spin, i.e., with a [541]1/2 proton and two $h_{11/2}$ neutron holes, while the latter corresponds to the configuration for the $h_{11/2}$ band, i.e., with no neutron holes and an odd $h_{11/2}$ proton. In the CNS calculations, the former configuration is clearly lowest in energy while the two configurations come at a similar energy in CNSB. This shows that the pairing energy is unusually strong in configurations with the odd proton in an $h_{11/2}$ orbital as noticed previously in Secs. III B and IV A 2.

The comparison between CNS and CNSB calculations for the $\varepsilon_2 \approx 0.30$ minimum shows that the deformation of this configuration is clearly smaller with pairing included, illustrating the general effect of pairing that it tends to reduce the shell effects; see, e.g., Fig. 14.5 of Ref. [46]. Coming back to Fig. 14, the calculated Q_t value for the large deformation minimum is thus considerably smaller with pairing included

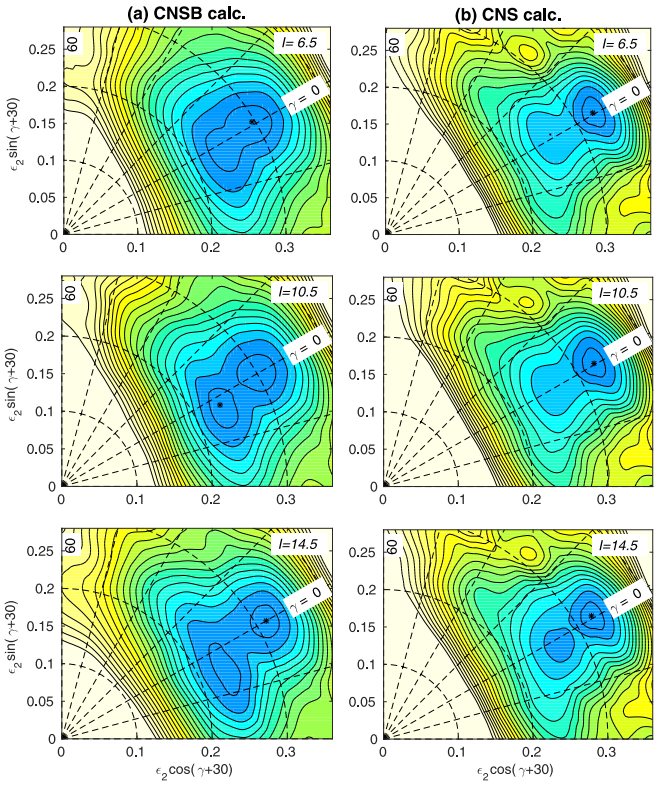

FIG. 15. Calculated total energy surfaces in the (ε_2, γ)-plane (a) with pairing included (CNSB) and (b) with no pairing (CNS) for the $(-, +1/2)(+, 0)$ configuration at spin values $I = 6.5$, 10.5 and 14.5. In each mesh point, the energy has been minimized with respect to ε_4 deformations. The contour line separation is 0.2 MeV.

but still much larger than experiment. However, the calculated value of Q_t for the small deformation minimum comes close to experiment. However, this minimum corresponds to the $h_{11/2}$ configuration and thus not to the [541]1/2 configuration which is assigned to negative parity yrast band at low spin. Coming back to this [541]1/2 configuration with no holes, its Q_t value calculated in CNS is larger than experiment but still reasonably close; see Fig. 14. As it does not show up as a local minimum in the energy surfaces of Fig. 15, we cannot easily calculate its value with pairing included. However, if the value is somewhat reduced by pairing in a similar way as for the $\pi([541]1/2)\nu(h_{11/2})^{-2}$ configuration, then it will come close to experiment. However, the way that bands 13a and band 14 cross at $I \approx 18$ strongly suggests that they have different configurations and thus that yrast band where Q_t has been measured, band 13a, has two $i_{13/2}$ holes for spin values below $I \approx 22$. The present calculations can be compared with the TRS calculations presented in Ref. [58]. They were done without keeping track of configurations. The fact that the calculated values came pretty close to the experiment indicates that the TRS yrast configuration has no $h_{11/2}$ holes.

The measured value for the band labeled as TSD1 is also shown in Fig. 14. The figure suggests that the values of Q_t for the TSD1 band and the 541 band are very similar. This appears strange as has been noted before; see Ref. [44]. One should note that the experimental values have an uncertainty

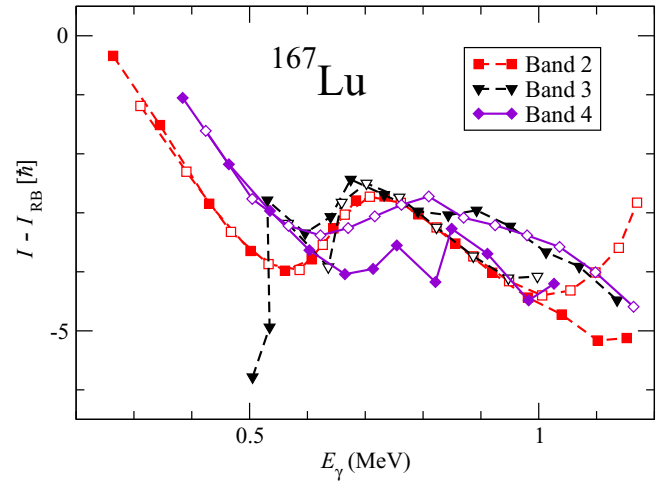

FIG. 16. The spin value with a rigid-body reference subtracted for the three-quasiparticle bands is shown versus the transition energy, E_γ.

of approximately 15% because of systematic errors. Therefore, it would be important to measure Q_t of the different normal-deformed and TSD bands in the same experiment in which case it should be possible to determine the relative values with a much better precision.

D. Three-quasiparticle (3qp) bands

1. The observed BC crossing in the 3qp configurations

The experimental bands 2, 3, and 4 are assigned as built on two quasineutrons and one quasiproton in Ref. [13]. A smooth crossing is observed in band 2 at the frequency $\hbar\omega = 0.32$ MeV with an alignment of 2–3$\hbar$. This is discussed in the Appendix where also plots of I versus E_γ with a rigid body reference subtracted were introduced. The bands 2, 3, and 4 are shown in such a diagram in Fig. 16. It is evident that all these bands go through a similar crossing, where the alignment is rather somewhat smaller for bands 3 and 4 and the crossing frequency (or E_γ) is somewhat larger in band 4 than in bands 2 and 3. The presence of this crossing, the $i_{13/2}$ BC crossing, and the absence of the AB crossing at a lower frequency shows that these bands have an odd number of $i_{13/2}$ neutrons, i.e., they can be assigned as three-quasiparticle configurations in agreement with Ref. [13]. We note that while the alignment in the AB crossing is quite large of the order of 8$\hbar$, it is much smaller in the BC crossing, namely, of the order 2$\hbar$. This is understood from the fact that one $i_{13/2}$ neutron is already aligned (and "blocked") in configurations which go through the BC crossing. The next crossing would then be the CD crossing in configurations with two aligned $i_{13/2}$ neutrons. Thus, this crossing is expected to be much less distinct that the BC crossing and it seems natural that it is not seen at all, in agreement with our conclusions in Sec. IV A.

2. Configurations of the 3qp bands which are calculated low in energy

The configurations of the favored three-quasiparticle bands can be read out from Fig. 3. Thus, the neutron $(i_{13/2})^5$

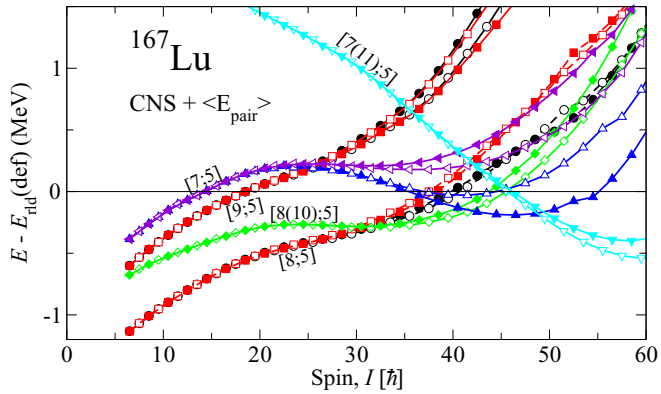

FIG. 17. Calculated "CNS + average pairing" energies for low-lying bands in ^{167}Lu with 9 hf and 5 $i_{13/2}$ neutrons.

configuration is combined with proton configurations with the odd particle in $\mathcal{N} = 4$ orbitals, in $h_{11/2}$, or in the hf orbital [541]1/2. The lowest calculated configurations of this type are drawn relative to the rotating liquid drop reference in Fig. 17. They are calculated in the CNS approach with an average pairing added. For spin values below $I \approx 30$, the lowest configuration has 8 $h_{11/2}$ protons and thus the odd proton in the [404]7/2 orbital. The orbitals of both the odd proton and the odd $\mathcal{N} = 5$ neutron are signature degenerate up to high frequencies so four bands, which are essentially overlapping in Fig. 17 up to $I \approx 30$, are formed. The calculated yrast states for $I \approx 30$–40 have the odd proton in the [541]1/2 orbital, where for the two bands drawn in Fig. 17, the favored $\alpha = 1/2$ signature of the [541]1/2 proton is combined with both signatures for the hf neutron. Bands with an odd number of $h_{11/2}$ protons are also calculated low in energy, where those with the odd proton in [523]7/2 (configuration [7;5]) and in [514]9/2 (configuration [9;5]) come at a similar energy at low spin as would be expected from Fig. 3, while the configuration with fewer $h_{11/2}$ protons is clearly favored at high spin. Indeed, it is this [7;5] configuration which is assigned to the observed positive parity band labeled 404h, which is yrast above $I \approx 30$. Finally, in Fig. 17 we have also added the lowest configuration with one proton in the $i_{13/2}$ orbital, [7(11);5]. Note that this configuration should be classified as having at least five quasiparticles because it has an odd proton in the $h_{11/2}$, hf, and $i_{13/2}$ orbitals in addition to the two odd neutrons. Configurations of this type are calculated to become yrast around $I = 50$, but because the position of the $i_{13/2}$ shell is not well established, this number is very uncertain. Several of the observed bands show discontinuities at the highest spin values. One possibility is that these discontinuities are caused by crossings with bands with one $i_{13/2}$ proton.

3. Comparison between observed and calculated 3qp configurations

The observed and calculated three-quasiparticle configurations are compared in Fig. 18. The bands 2 and 3 could be assigned to the four [8;5] configurations drawn in Fig. 17. However, there is also the possibility to form excited CNS bands, i.e., the second or third lowest band within some CNS

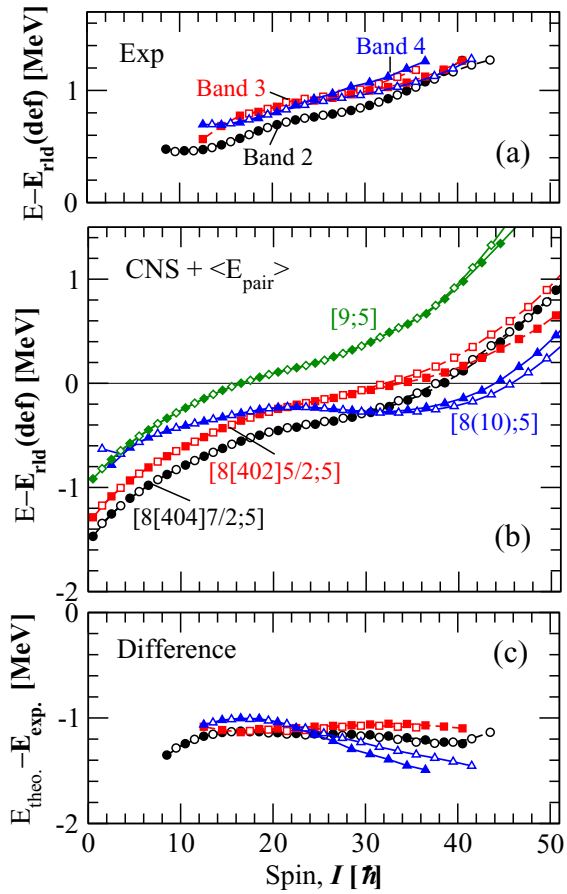

FIG. 18. Experimental energies (a) and theoretical "CNS + average pairing" energies (b) relative to a rotating liquid drop and their differences (c) as a function of spin for bands 2, 3, and 4 in ^{167}Lu.

configurations. Such configurations were previously considered for the $\mathcal{N} = 4$ positive parity bands. In an analogous way, in the [8;5] bands drawn in Fig. 17, the odd proton is placed in the [404]7/2 orbital but it can be lifted to the [402]5/2 orbital at a low energy cost. Thus, the two lowest bands with the odd proton in [404]7/2 and [402]5/2, respectively, are drawn in Fig. 18 and compared with the observed bands 2 and 3. The difference between calculations comes out as rather constant around −1 MeV which clearly supports this interpretation. The fact that the observed bands are split by approximately 200 keV at low spin makes this interpretation more plausible than the assumption that bands 2 and 3 are built on the four [8;5] bands shown in Fig. 17. However, one should also note that there will be some residual interaction between the bands, i.e., the observed bands should rather be assigned to some mixture of the pure CNS bands. Such mixing, however, will only have some minor influence on the energies and will not really be noticed on the energy scales used in Fig. 18.

The interpretation of bands 2 and 3 as [8;5] is further supported by the comparison with the corresponding paired configuration, i.e., the lowest $(+, \pm 1/2)(-, 1)$ in Fig. 11. Note that the difference curve for band 2 comes close to that for the $h_{11/2}$ band and that the spin dependence for the two difference curves in the lower panel of Fig. 11 is very similar.

As seen in Fig. 17, among three-quasiparticle configurations with positive parity, [8(10);5] is the lowest one for spins $I < 40$. This suggests that band 4 should be assigned to this configuration. One might also argue that the crossing for signature $\alpha = -1/2$ between band 4 and bands 2 and 3 at spin $I \approx 30$ is reproduced for the configurations [8(10);5] and [8;5]. However, considering the overall features, it is evident that the observed bands 2, 3, and 4 have a rather similar spin dependence while for the calculated bands, the [8(10);5] configuration comes down a few hundred keV relative to [8;5] in the spin range $I \approx 15$–40. In Fig. 17, it appears that the energy curve for the [9;5] configuration is more parallel to that of the [8;5] configuration in general agreement with the behavior of bands 2, 3, and 4. This would suggest that band 4 should rather be assigned to the [9;5] configuration as done on Ref. [13]. However, considering the differences in detail, it turns out that the calculated energy curve of the configuration [9;5] comes up too steep at high spin leading to a difference between calculations and experiment (not shown in Fig. 18) which increases in an unrealistic way. Thus, the assignment of band 4 to the [8(10);5] configuration is well motivated.

A final observation for the three-quasiparticle bands is that one would expect to observe the [7;5] configuration because in Fig. 17, it is clearly calculated lowest in energy for $I = 40$–50. It has no correspondence among the observed low-lying bands labeled as "3qp", but instead, in Sec. IV A, it was assigned to the positive parity band which is yrast for $I \approx 30$–50, the 404h band. The fact that no other observed band is naturally assigned to the [7;5] configuration gives a strong support to our assignment for the 404h band.

V. SUMMARY AND CONCLUSIONS

We have employed the unpaired CNS and paired CNSB formalisms to determine the structure of the observed rotational bands in ^{167}Lu. It turns out that the configurations calculated with pairing included are well described in the unpaired formalism if an average pairing energy is added. Thus, the more detailed configuration assignment in the unpaired formalism in terms of number of particles in different j shells or groups of j shells can be used to classify the observed bands. This is possible even though some features show up only in the paired formalism, especially the low energy in the $(\pi, \alpha) = (+, 0)$ neutron configurations below the first $(i_{13/2})^2$ backbend at $I = 12$–14, the AB crossing. Also in configurations with an odd number of $i_{13/2}$ neutrons, the paired $(i_{13/2})^2$ crossing, the BC crossing, is seen for spin values $I = 15$–20, but the alignment is so small that its contribution to the total energy is almost negligible. Furthermore, the full pairing calculation is important in an extended spin range for one-quasiparticle configurations with the odd proton in an orbital far away from the Fermi surface.

Some positive parity bands which interact are redefined into structures which evolve smoothly with spin, where approximate interaction strengths between these structures are extracted. Some previous configuration assignments are confirmed, while the interpretation of some experimental bands and also the origin of the crossings are revised. For ^{167}Lu with an odd number of protons, the low spin one-quasiparticle configurations are followed at somewhat higher spin values by three-quasiparticle configurations with an odd number of hf and $i_{13/2}$ neutrons. Note, however, that at high spin, say $I > 30$, the division into configurations with a fixed number of quasiparticles is not meaningful because, with weaker pairing correlations, the different spin vectors will align gradually; i.e., the spin vectors of all valence particles will be partially aligned.

In our interpretation, those configurations which would be expected to come low in energy according to a single-routhian diagram, see Fig. 3, have all been localized in the observed level scheme. Similarly, reasonable interpretations have been found to all low-lying bands which are observed in an extended spin range.

Considering our preferred assignments, the extension of the [404]7/2 band after the band-crossing at $I \approx 30$ is assigned as a three-quasiparticle configuration with negative parity for both protons and neutrons, while the smooth continuation of the [404]7/2 band is observed as nonyrast up to $I \approx 40$. In the observed $h_{11/2}$ band, the band-crossing at $I = 40$ is caused by the occupation of the lowest $h_{9/2}$ orbital, [541]1/2. This $h_{9/2}$ orbital is assigned to the band-head of a one-quasiparticle configuration which comes low in energy because of an increased deformation caused by two $h_{11/2}$ neutron holes. In this band, there is a band-crossing at $I \approx 20$, where the configuration with no $h_{11/2}$ holes comes lower in energy. The positive parity three-quasiparticle band is assigned as built on a configuration with one $h_{9/2}$ proton. In general, the relative energy of bands assigned as having one $h_{9/2}$ proton and no $h_{9/2}$ proton, respectively, agrees with experiment. This fact indicates that the proton $h_{9/2}$ shell situated above the $Z = 82$ gap is placed at a proper energy with present single-particle parameters.

We have not tried to interpret the band which is assigned as TSD; i.e., "triaxial strongly deformed." However, we have noticed the strange feature that this TSD band interacts strongly with one or several normal-deformed bands at $I \approx 30$ and tried to extract the interaction strength. A problem is, however, that bands which appear to interact with the TSD band are observed only for spin values below the interaction region. It would thus be important to follow these bands in experiment through the interaction region.

Measurements of the lifetimes in the TSD band and the yrast ND band have been presented [58,59]. However, these life-times are associated with large uncertainties and appear somewhat confusing when compared with the present calculations. Thus, it would be important to carry out lifetime experiment for several bands including the TSD band in the same experiment, which should make it possible to determine at least the relative lifetimes with a much better accuracy.

Our calculations are limited to one nucleus but should be valid in general not only for the rotational bands in the deformed rare-earth region but also for high-spin states in other mass regions. This concerns, for example, the observation that "paired band crossings" are mainly seen at low spin and absent in the very high spin region, and the conclusion that after the first or possibly second band crossing, high-spin states should not be classified by the number of quasiparticles but rather by the distribution of particles over the different

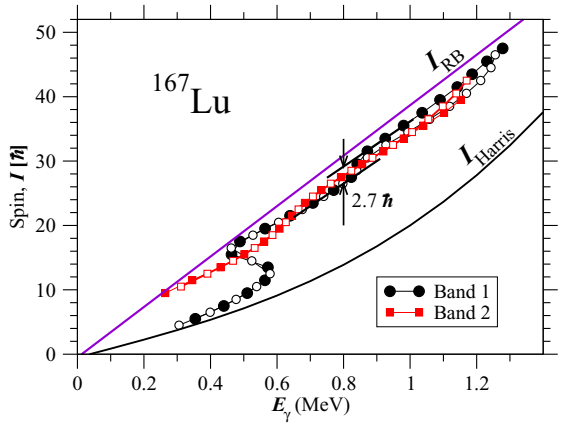

FIG. 19. Spin I versus transition energy E_γ for the bands labeled 1 and 2 in Ref. [13], see Fig. 17 in that reference. Furthermore, the rigid body spin, $I_{\rm RB}$, and the spin according to Harris' formula [61], $I_{\rm Harris} = \omega\mathcal{J}_0 + \omega^3\mathcal{J}_1$ ($\mathcal{J}_0 = 27\hbar^2{\rm MeV}^{-1}$, $\mathcal{J}_1 = 56\hbar^4{\rm MeV}^{-3}$) are drawn.

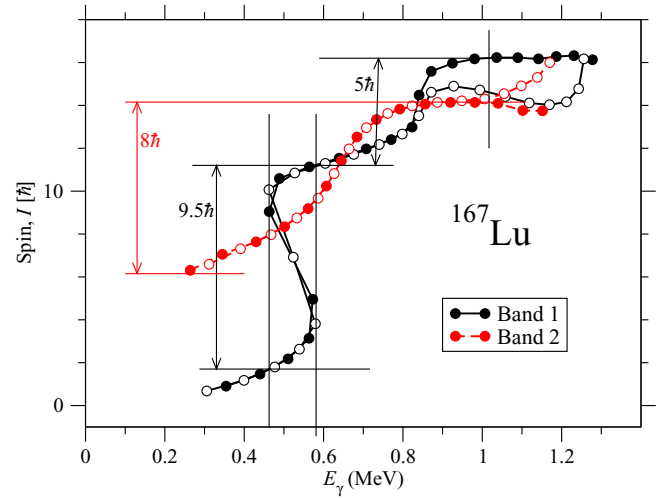

FIG. 20. The spin I relative to $I_{\rm Harris}$ with $\mathcal{J}_0 = 27\hbar^2{\rm MeV}^{-1}$ and $\mathcal{J}_1 = 56\hbar^4{\rm MeV}^{-3}$ for the same bands as in Fig. 19. Lines are drawn to show how the alignments listed in Table III of Ref. [13] can be obtained.

j shells or groups of j shells. The present study is the first one where the CNS and CNSB methods have been combined to describe a large number of rotational bands for a nucleus in the deformed rare-earth region, but previous studies of the transitional nucleus ^{161}Lu [24] or on the yrast bands in $^{168-175}$Hf [60] support that our conclusions can be considered to be a more general nature.

ACKNOWLEDGMENTS

H.-L.M. acknowledges the support from the NSF of China under Contracts No. 11105227 and No. 11205245.

APPENDIX: BAND CROSSINGS AND ALIGNED SPIN

Much of the analysis of high-spin bands has been based on band-crossings, where these crossings are often assumed to be caused by pairing. For such crossings, the alignment is an important quantity when comparing experiment and calculations. However, different definitions of the alignment have been used in the litterature. Especially, it appears that the definition used in Ref. [13] is different from the one we use. In view of this, we will give some comments on how band crossings can be analyzed and consider in some detail the crossings seen in the bands labeled as 1 and 2 in Ref. [13]. Thus, in Fig. 19 the spin I of these bands is plotted versus the transition energy, E_γ. Note that we define the rotational frequency as $\hbar\omega = E_\gamma/2$, i.e., $\hbar\omega$ is half the transition energy, so it is equivalent to plot I versus ω. Furthermore, because we are mainly interested in high spin states, we identify the total spin with its projection on the rotation axis, $I \equiv I_x$.

Let us first concentrate on the second crossing in the $\alpha = +1/2$ branch of band 1, i.e., the crossing which was analyzed in connection with Fig. 2(b). To find out how much spin is gained in this crossing, we draw two parallel lines following the transitions below and above the crossing and can conclude that the lines are displaced by approximately $2.7\hbar$. The conclusion is thus that in addition to the smooth spin increase from the core, $2.7\hbar$ is gained from the change of the wave-function at the crossing. This change could either be caused by the alignment of a pair of high-j particles or a change of the orbital occupation.

In the analysis of band crossings, a reference spin $I_{\rm ref}$ is often subtracted from the total spin where this reference is generally chosen from the parametrization of Harris [61], $I_{\rm ref} = \omega\mathcal{J}_0 + \omega^3\mathcal{J}_1$. The idea is then to choose the constants $\mathcal{J}_0$ and $\mathcal{J}_1$ such that the reference spin follows the smooth raise of the I versus ω (or I versus E_γ) curve before and after the crossing, i.e., I-$I_{\rm ref}$ will be approximately constant outside the band crossing region [4]. However, it is in general difficult to find constants $\mathcal{J}_0$ and $\mathcal{J}_1$ so that this constancy is fulfilled in the entire spin range. Consider, e.g., the constants chosen in Ref. [13] where the corresponding reference spin, $I_{\rm Harris}$, is shown in Fig. 19 while the I-$I_{\rm Harris}$ curves for bands 1 and 2 are shown in Fig. 20. It appears that in this case, the constants have been chosen such that the I-$I_{\rm ref}$ curves become constant at high transition energies, $E_\gamma \approx 0.8$–1.2 MeV. Then, even though the curves are not constant outside band crossing regions at smaller values of E_γ, it is assumed that $I_{\rm ref}$ represents the smooth average increase of the spin, i.e., that the full spin of the I-$I_{\rm ref}$ curve is built from alignments at band-crossings. There is still some arbitrariness about over which E_γ range the different alignments should be counted. However, if it is assumed that for a full backbend only the frequency region (or E_γ region) covering the backbend should be counted, then the alignment at the different crossings of the $\alpha = 1/2$ bands can be extracted using the lines drawn in Fig. 20. Thus, alignments of $9.5\hbar$ and $5\hbar$ can be read out from the first and second band crossings in band 1 and $8\hbar$ for the crossing at $E_\gamma \approx 0.64$ MeV in band 2.

A problem with the definition of the spin alignment used in Ref. [13] is that it will depend on the $I_{\rm ref}$ curve which is subtracted. For example, in the previous study of high spin states in ^{167}Lu [53], the constants $\mathcal{J}_0$ and $\mathcal{J}_1$ were chosen such

that the I-$I_{\rm ref}$ curve became essentially constant before and after the first band-crossing of band 1. The alignment at this crossing was then extracted as $8.5\hbar$. This value is consistent with the value we get if parallel lines are drawn in Fig. 19 in a similar way as for the second crossing. The conclusion is that only if an $I_{\rm ref}$ curve can be defined which makes I-$I_{\rm ref}$ essentially constant in some E_γ (or ω) region both before and after the crossing, this is consistent way to define the aligned spin.

It can be helpful to subtract some reference from the I versus E_γ curve to see the different discontinuities more clearly. When considering the full spin range up to $I \approx 50$, it is evident that the spin I is roughly proportional to E_γ; see Fig. 19. Then, the strategy is to choose the reference such that the differences from this straight line behavior are highlighted. Different possibilities which in practice are very similar are to choose $\mathcal{J}_1 = 0$ in the Harris formula or to use some reference of rigid body type, where the latter option appears more natural in connection with the present CNS and CNSB calculations. The behavior will be similar if the rigid body moment of inertia is calculated at a fixed deformation or alternatively calculated at the minimum energy of the rotating liquid drop energy as in our standard reference energy [9]; see, e.g., Figs. 1 and 2. With the rigid body constants chosen according to Eq. (70) in Ref. [18], $I_{\rm RB}$ comes out as in Fig. 19, while I-$I_{\rm RB}$ is drawn versus E_γ for bands 1 and 2 in Fig. 21. It is now easy to read out that the alignment at the second crossing of band 1 is approximately $2.5\hbar$. If the parallel lines are drawn as in Fig. 19, i.e., following the trend of a few transitions before and after the crossing, then we will of course get the same answer, $2.7\hbar$, according to the lines drawn. If the points closest to the crossing is given a higher weight, i.e., lines which come closer to a constant value of I-$I_{\rm RB}$, then we will get somewhat smaller values of the alignment, down to ≈ 2.2–$2.3\hbar$. Thus, it is difficult to define a very precise value of the alignment. However, a value which is precise enough for the theoretical analysis can easily be deduced either from the I versus E_γ plot or from the plot with $I_{\rm RB}$ subtracted from the spin I.

Let us come back to the small alignment of band 2 at $E_\gamma \approx 0.65$ MeV. This alignment is almost invisible in the I versus E_γ plot in Fig. 19. However, it shows up clearly in Fig. 21

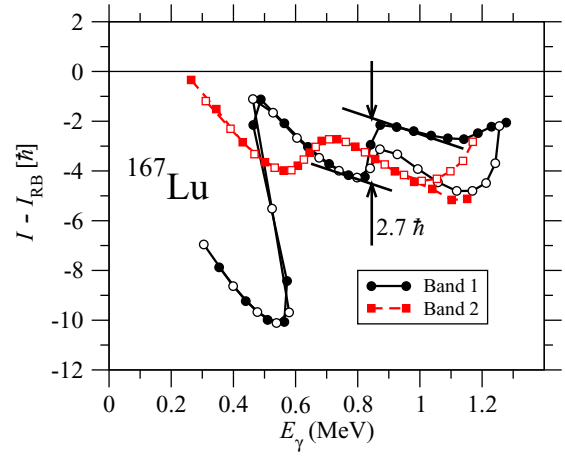

FIG. 21. The spin relative to $I_{\rm RB}$ is drawn versus E_γ for the same bands as in Figs. 19 and 20. In an analogous way as in Fig. 19, lines are drawn to indicate how an alignment of $2.7\hbar$ can be obtained for the second crossing in band 1.

when $I_{\rm RB}$ is subtracted, where one can easily get a rough estimate of approximately $2\hbar$ for the alignment. Note that in this case, an alignment of $8\hbar$ was deduced in Ref. [13]; see Fig. 20. Note also that it is not easy to extract the alignment at this crossing according to our definitions from Fig. 20. It appears that this is because of the ω^3 term which results in a curvature in the $I_{\rm Harris}$ function. Especially, going to very high spins, the ω^3 term will dominate making this reference unrealistic.

Summarizing, it is evident that depending on definitions, very different values can be deduced for the alignment at a band-crossing. However, if we accept that the alignment should measure the additional spin which is gained at a band-crossing, then the uncertainties become much smaller and the value can easily be determined with an acceptable accuracy. For example, to extract the alignment for the first back-bending, the method to subtract a reference $I_{\rm ref}$ based on Harris formula will give well-defined values as long as the parameters of the reference are fitted for this specific spin range. However, to extract alignments at different spin values up to high spins, a reference of rigid body type appears more suitable.

[1] A. Johnson, H. Ryde, and S. Hjorth, Nucl. Phys. A **179**, 753 (1972).
[2] F. S. Stephens, Rev. Mod. Phys. **47**, 43 (1975).
[3] A. Bohr and B. R. Mottelson, Proc. Int. Conf. Nuclear Structure, Tokyo (1977) [Jpn. J. Phys., Suppl. **44**, 157 (1978)].
[4] R. Bengtsson and S. Frauendorf, Nucl. Phys. A **314**, 27 (1979); **327**, 139 (1979).
[5] L. L. Riedinger, Phys. Scr. **24**, 312 (1981).
[6] M. J. A. de Voigt, J. Dudek, and Z. Szymański, Rev. Mod. Phys. **55**, 949 (1983).
[7] T. Bengtsson and I. Ragnarsson, Nucl. Phys. A **436**, 14 (1985).
[8] I. Ragnarsson, V. P. Janzen, D. B. Fossan, N. C. Schmeing, and R. Wadsworth, Phys. Rev. Lett. **74**, 3935 (1995).
[9] B. G. Carlsson and I. Ragnarsson, Phys. Rev. C **74**, 011302(R) (2006).
[10] T. Bengtsson, Nucl. Phys. A **496**, 56 (1989).
[11] T. Bengtsson, Nucl. Phys. A **512**, 124 (1990).
[12] A. Axelsson, R. Bengtsson, and J. Nyberg, Nucl. Phys. A **708**, 226 (2002).
[13] D. G. Roux, W. C. Ma, G. B. Hagemann, H. Amro, D. R. Elema, P. Fallon, A. Görgen, B. Herskind, H. Hübel, Y. Li *et al.*, Phys. Rev. C **92**, 064313 (2015).
[14] I. Ragnarssson, S. Åberg, and R. K. Sheline, Phys. Scr. **24**, 215 (1981).
[15] C. E. Svensson, A. O. Macchiavelli, A. Juodagalvis, A. Poves, I. Ragnarsson, S. Åberg, D. E. Appelbe, R. A. E. Austin, G. C. Ball, M. P. Carpenter *et al.*, Phys. Rev. C **63**, 061301(R) (2001).

[16] J. Gellanki, D. Rudolph, I. Ragnarsson, L-L. Andersson, C. Andreoiu, M. P. Carpenter, J. Ekman, C. Fahlander, E. K. Johansson, A. Kardan *et al.*, Phys. Rev. C **86**, 034304 (2012).
[17] J. J. Valiente-Dobón, T. Steinhardt, C. E. Svensson, A. V. Afanasjev, I. Ragnarsson, C. Andreoiu, R. A. E. Austin, M. P. Carpenter, D. Dashdorj, G. de Angelis *et al.*, Phys. Rev. Lett. **95**, 232501 (2005).
[18] A. V. Afanasjev, D. B. Fossan, G. J. Lane, and I. Ragnarsson, Phys. Rep. **322**, 1 (1999).
[19] K. Starosta, C. J. Chiara, D. B. Fossan, T. Koike, D. R. La Fosse, G. J. Lane, J. M. Sears, J. F. Smith, A. J. Boston, P. J. Nolan *et al.*, Phys. Rev. C **64**, 014304 (2001).
[20] I. Ragnarsson, Nucl. Phys. A **557**, 167 (1993).
[21] A. O. Evans, E. S. Paul, J. Simpson, M. A. Riley, D. E. Appelbe, D. B. Campbell, P. T. W. Choy, R. M. Clark, M. Cromaz, P. Fallon *et al.*, Phys. Rev. C **73**, 064303 (2006).
[22] J. Simpson, M. A. Riley, S. J. Gale, J. F. Sharpey-Schafer, M. A. Bentley, A. M. Bruce, R. Chapman, R. M. Clark, S. Clarke, J. Copnell *et al.*, Phys. Lett. B **327**, 187 (1994).
[23] B. G. Carlsson, I. Ragnarsson, R. Bengtsson, E. O. Lieder, R. M. Lieder, and A. A. Pasternak, Phys. Rev. C **78**, 034316 (2008).
[24] H.-L. Ma, B. G. Carlsson, I. Ragnarsson, and H. Ryde, Phys. Rev. C **90**, 014316 (2014).
[25] P. Bringel G. B. Hagemann, H. Hübel, A. Al-khatib, P. Bednarczyk, A. Bürger, D. Curien, G. Gangopadhyay, B. Herskind, D. R. Jensen *et al.*, Eur. Phys. J. A **24**, 167 (2005).
[26] D. R. Jensen, G. B. Hagemann, I. Hamamoto, S. W. Ødegård, M. Bergström, B. Herskind, G. Sletten, S. Törmänen, J. N. Wilson, P. O. Tjøm *et al.*, Nucl. Phys. A **703**, 3 (2002).
[27] G. Schönwaßer, H. Hübel, G. B. Hagemann, P. Bednarzyk, G. Benzoni, A. Bracco, P. Bringel, R. Chapman, D. Curien, J. Domscheit, B. Herskind *et al.*, Phys. Lett. B **552**, 9 (2003).
[28] H. Amro, W. C. Ma, G. B. Hagemann, R. M. Diamond, J. Domscheit, P. Fallon, A. Görgen, B. Herskind, H. Hübel, D. R. Jensen *et al.*, Phys. Lett. B **553**, 197 (2003).
[29] P. Bringel, H. Hübel, A. Al-Khatib, A. Bürger, N. Nenoff, A. Neusser-Neffgen, G. Schönwaßer, A. K. Singh, G. B. Hagemann, B. Herskind *et al.*, Phys. Rev. C **73**, 054314 (2006).
[30] D. R. Jensen, G. B. Hagemann, I. Hamamoto, B. Herskind, G. Sletten, J. N. Wilson, S. W. Ødegård, K. Spohr, H. Hübel, P. Bringel *et al.*, Eur. Phys. J. A **19**, 173 (2004).
[31] P. Bringel, C. Engelhardt, H. Hübel, A. Neusser-Neffgen, S. W. Ødegård, G. B. Hagemann, C. R. Hansen, B. Herskind, G. Sletten, M. P. Carpenter *et al.*, Phys. Rev. C **75**, 044306 (2007).
[32] G. Schönwaßer, N. Nenoff, H. Hübel, G. B. Hagemann, P. Bednarczyk, G. Benzoni, A. Bracco, P. Bringel, R. Chapman, D. Curien *et al.*, Nucl. Phys. A **735**, 393 (2004).
[33] J. C. Marsh, W. C. Ma, G. B. Hagemann, R. V. F. Janssens, R. Bengtsson, H. Ryde, M. P. Carpenter, G. Gürdal, D. J. Hartley, C. R. Hoffman *et al.*, Phys. Rev. C **88**, 041306(R) (2013).
[34] R. B. Yadav, W. C. Ma, G. B. Hagemann, H. Amro, A. Bracco, M. P. Carpenter, J. Domscheit, S. Frattini, D. J. Hartley, B. Herskind *et al.*, Phys. Rev. C **80**, 064306 (2009).
[35] H. Schnack-Petersen, R. Bengtsson, R. A. Bark, P. Bosetti, A. Brockstedt, H. Carlsson, L. P. Ekström, G. B. Hagemann, B. Herskind, F. Ingebretsen *et al.*, Nucl. Phys. A **594**, 175 (1995).
[36] R. Bengtsson and H. Ryde, Eur. Phys. J. A **22**, 355 (2004).
[37] B. G. Carlsson, Int. J. Mod. Phys. E **16**, 634 (2007).
[38] A. Kardan, I. Ragnarsson, H. Miri-Hakimabad, and L. Rafat-Motevali, Phys. Rev. C **86**, 014309 (2012).
[39] I. Hamamoto and G. B. Hagemann, Phys. Rev. C **67**, 014319 (2003).
[40] Y. R. Shimizu, T. Shoji, and M. Matsuzaki, Phys. Rev. C **77**, 024319 (2008).
[41] K. Sugawara-Tanabe and K. Tanabe, Phys. Rev. C **82**, 051303(R) (2010).
[42] D. Almehed, F. Dönau, and S. Frauendorf, Phys. Rev. C **83**, 054308 (2011).
[43] S. Frauendorf and F. Dönau, Phys. Rev. C **92**, 064306 (2015).
[44] I. Ragnarsson, Phys. Scr. **92**, 124004 (2017).
[45] R. Wadsworth, I. Ragnarsson, B. G. Carlsson, Hai-Liang Ma, P. J. Davies, C. Andreoiu, R. A. E. Austin, M. P. Carpenter, D. Dashdorj, S. J. Freeman *et al.*, Phys. Lett. B **701**, 306 (2011).
[46] S. G. Nilsson and I. Ragnarsson, *Shapes and Shells in Nuclear Structure* (Cambridge University Press, Cambridge, England, 1995).
[47] V. Strutinsky, Nucl. Phys. A **95**, 420 (1967).
[48] K. Pomorski and J. Dudek, Phys. Rev. C **67**, 044316 (2003).
[49] I. Ragnarsson, B. G. Carlsson, A. Kardan, and H. Ma, Acta Phys. Polo. B **46**, 477 (2015).
[50] A. Juodagalvis, I. Ragnarsson, and S. Åberg, Phys. Lett. B **477**, 66 (2000).
[51] X. Wang, M. A. Riley, J. Simpson, E. S. Paul, J. Ollier, R. V. F. Janssens, A. D. Ayangeakaa, H. C. Boston, M. P. Carpenter, C. J. Chiara *et al.*, Phys. Lett. B **702**, 127 (2011).
[52] R. V. F. Janssens, M. J. A. de Voigt, H. Sakai, H. J. M. Aarts, C. J. Van der Poel, H. F. R. Arciszewski, D. E. C. Scherpenzeel, and J. Vervier, Phys. Lett. B **106**, 475 (1981).
[53] C.-H. Yu, G. B. Hagemann, J. M. Espino, K. Furuno, J. D. Garrett, R. Chapman, D. Clarke, F. Khazaie, J. C. Lisle, J. N. Mo *et al.*, Nucl. Phys. A **511**, 157 (1990).
[54] T. Bengtsson and I. Ragnarsson, Phys. Lett. B **163**, 31 (1985).
[55] S. Ogaza, J. Kownacki, M. P. Carpenter, J. Gascon, G. B. Hagemann, Y. Iwata, H. J. Jensen, T. Komatsubara, J. Nyberg, G. Sletten *et al.*, Nucl. Phys. A **559**, 100 (1993).
[56] D. J. Hartley, W. H. Mohr, J. R. Vanhoy, M. A. Riley, A. Aguilar, C. Teal, R. V. F. Janssens, M. P. Carpenter, A. A. Hecht, T. Lauritsen *et al.*, Phys. Rev. C **74**, 054314 (2006).
[57] H. J. Jensen, R. A. Bark, P. O. Tjøm, G. B. Hagemann, I. G. Bearden, H. Carlsson, S. Leoni, T. Lönnrot, W. Reviol, L. L. Riedinger *et al.*, Nucl. Phys. A **695**, 3 (2001).
[58] A. Rohilla, R. P. Singh, S. Muralithar, A. Kumar, I. M. Govil, and S. K. Chamoli, Phys. Rev. C **100**, 024325 (2019).
[59] H. Gürdal, H. Amro, C. W. Beausang, D. S. Brenner, M. P. Carpenter, R. F. Casten, C. Engelhardt, G. B. Hagemann, C. R. Hansen, D. J. Hartley *et al.*, J. Phys. G: Nucl. Part. Phys. **31**, S1873 (2005).
[60] H. Taheri, A. Kardan, and M. H. Hadizadeh Yazdi, Phys. Rev. C **98**, 054313 (2018).
[61] S. M. Harris, Phys. Rev. **138**, B509 (1965).